

Investigation of Bit-Rock Interaction for Rotary Drilling and Influence on Penetration Rate

by

© Jinghan Zhong

A Thesis submitted to the

School of Graduate Studies

in partial fulfillment of the requirements for the degree of

Master of Engineering

Faculty of Engineering and Applied Science

Memorial University of Newfoundland

Table of Contents

| | |
|--|------|
| Abstract..... | iv |
| Acknowledgement | vi |
| List of Abbreviations, Nomenclature and Symbols..... | viii |
| List of Table..... | x |
| List of Figures | xi |
| Chapter 1 Introduction | 1 |
| 1.1 Research Background..... | 1 |
| 1.2 Research Purpose and Objectives | 2 |
| 1.3 Significance Process of Research..... | 2 |
| Chapter 2 Literature Review..... | 6 |
| 2.1 Penetration Mechanism of PDC bits | 6 |
| 2.1.1 Research and development of polycrystalline diamond compacts (PDC) | 6 |
| 2.1.2 The role of single PDC cutters in rock stress analysis | 7 |
| 2.1.3 Analysis of the rock cutting mechanism..... | 10 |
| 2.2 PWARD Drilling Tools | 11 |
| 2.3 Distinct Element Method (DEM)..... | 12 |
| 2.4 Cutter-Rock interaction..... | 14 |
| Chapter 3 Distinct Element Method (DEM) modeling of the Cutter Parameters..... | 16 |
| 3.1 Brief Description of PFC2D Software | 16 |
| 3.1.1 PFC2D Rock-Cutting Environment..... | 16 |
| 3.2 Simulation of drilling rock, microscopic and macroscopic Properties | 19 |
| 3.3 Simulating on Single Cutter Penetration Considerations and Input Parameters..... | 22 |

| | |
|--|----|
| Chapter 4 Investigated Lab PWARD Tools and Operational Mechanism with Discrete Element Method (DEM) Modeling of the Lab Scale Tool | 24 |
| 4.1 Introduction | 25 |
| 4.2 Experimental Setup | 26 |
| 4.2.1 Test Materials | 27 |
| 4.2.2 Small Drilling Simulator | 27 |
| 4.2.3 Monitoring Acoustic Emission..... | 28 |
| 4.2.4 Cutting Analysis Overview | 30 |
| 4.3 Results | 30 |
| 4.3.1 Review of Drilling Conditions | 31 |
| 4.3.2 Rock Penetration Characterization | 31 |
| 4.3.3 Cutting Analysis Results | 33 |
| 4.3.4 Acoustic Emission Results | 37 |
| 4.3.5 Acoustic Emission and ROP..... | 39 |
| 4.4 Discussion and Conclusions..... | 40 |
| Chapter 5 DEM Simulation of Enhancing Drilling Penetration Using Vibration and Experimental Validation..... | 42 |
| 5.1 Introduction | 43 |
| 5.2 Laboratory Drill-Off Tests | 45 |
| 5.2.1 Drilling Tests | 45 |
| 5.3 Numerical Simulation | 48 |
| 5.3.1 Material Calibration..... | 48 |
| 5.3.2 Model Construction | 50 |
| 5.3.3 Simulation Results | 52 |
| 5.4 Conclusions | 55 |

| | |
|--|----|
| Chapter 6 Characterization of the Dynamic Compliance for the Passive Vibration Assisted Rotation Drilling (pVARD) Tool..... | 56 |
| 6.1 Introduction..... | 57 |
| 6.1.1 Experiment Setup and Materials of Equipment..... | 58 |
| 6.2 Analysis and Conclusion..... | 73 |
| Chapter 7 DEM Modeling of the PWARD Drilling Under Field Conditions | 75 |
| 7.1 Field Trial Summary | 75 |
| 7.2 DEM Input Data | 80 |
| 7.3 DEM Simulation Results..... | 81 |
| Chapter 8 Conclusion and Future Work | 86 |
| 8.1 Summary and Conclusion | 86 |
| 8.1.1 Axial Compliance and Effect of PWARD Tool | 87 |
| 8.1.2 Conclusion | 87 |
| 8.2 Future work | 88 |
| Appendix A..... | 89 |
| MSE and MRR and Average ROP Calculation | 89 |
| REFERENCES | 92 |

Abstract

In this thesis a comprehensive investigation of non-natural vibration on enhanced drilling performance is studied. The Drilling Technology Laboratory (DTL) at Memorial University of Newfoundland has been working on a passive Vibration Assisted Rotational Drilling (p-VARD) tool which helps to increase the drilling rate of penetration (ROP) during laboratory testing and field work for this couple of years. It has been proven by laboratory experiments and field work that axial vibration can play a dramatically positive role in improving drilling ROP. Meanwhile, the laboratory measurement and field trial results show that the new passive vibration tool with sensor-sub can provide compatible and accurate data to identify drill string motions including rotatory speed, bit orientation, and bit vibrations including axial, lateral, torsional vibrations and bit whirl. These raw data from each drilling experiment can supply a sufficient research basis for numerical simulation.

This thesis focuses on the effect of axial vibration on polycrystalline diamond compact (PDC) bit drilling performance using Discrete Element Method (DEM) simulation and experiments with the new vibration tool. Drill-off tests were conducted in the laboratory with axial vibration on the drill string. Vibration properties were adjusted by different settings of spring compliance and dampening layers. In order to study the cutting performance of the new tool, a PFC2D (Particle Flow Code in 2 Dimensions) numerical model was developed to simulate the micro-crack generation and propagation during the drilling process in synthetic rock samples. This experimental data was used to calibrate this numerical model to real drilling situations. The analyses of the Mechanic Specific Energy (MSE), the Material Removal Rate (MRR) and the Depth of Cut (DOC) are compared with a non-vibration case to evaluate ROP and drilling

efficiency. The simulations result demonstrated significant increase in drilling performance when the p-VARD tool was used in the process. Simulation results of the two types of conditions of tools were analyzed and compared in lab and field work experiment respectively. The experimental data agrees with numerical simulation results which indicate it as a promising method to simulate PDC cutter-rock interaction with DEM modelling using the new pVARD tool.

Acknowledgement

I would like to express my genuine gratitude to a number of people who help me to continue my research, finish my thesis and have a new life in Canada. I would like to give all thanks and appreciate to all people below:

Thanks to my academic supervisor, Professor Stephen Butt, who funding my research, providing me with patient guidance in experimental work, direction of my simulation and thesis preparation, great training, courses and other experiences that I have gained when studying at Memorial University of Newfoundland. Without him, anything is impossible for my research and study in Canada.

Thanks to my co-supervisor, Dr. Jianming Yang, who give me many advices and encouragement to my research and spirits. If not his support, I will depression and I will never know how to do with the mechanical part of my research. His ideas about my mechanics work helped me a lot in deciding different simulation scenarios and parameters.

Thanks to my family who supported me through my entire life. Without their encouragement and support I have never managed to complete this research and I will get nothing in the life.

Thanks to my friends and Project Manager, HongyuanQiu, Yingjian Xiao and Pushpinder for their great support and guidance throughout my Master's degree. Their countless effort in assisting me with data analyses and providing useful information is appreciated. In addition, thanks to Igor Kyzym and Rosana Reyes for their great help laboratory experiments.

Thanks to my colleagues, Mohammad Mozaffariand Yousef Gharibiyamchi for their help and ideas in programming the simulations. Without their help, this work would never been completed.

Thanks to all members of Advanced Drilling Group for their cooperation, support, and friendly environment. Special thanks to Brock and Qian Gao.

The project is funded by Atlantic Canada Opportunity Agency (AIF contract number: 781-2636-1920044), involving Husky Energy, Suncor Energy and Research and Development Corporation (RDC) of Newfoundland and Labrador. Many thanks will be given to all of them.

List of Abbreviations, Nomenclature and Symbols

| | |
|-------------|---|
| CCS | Confined Compressive Strength |
| DEM | Distinct Element Method |
| DTL | Drilling Technology Laboratory |
| DOC | Depth of Cut |
| IADC | International Association of Drilling Contractors |
| MRR | Material Removal Rate |
| MSE | Mechanical Specific Energy |
| PDC | Polycrystalline Diamond Compact |
| PVARD Tools | Passive Vibration Assisted Rotational Drilling (VARD) Tools |
| PFC | Particle Flow Code |
| ROP | Rate of Penetration |
| RPM | Revolution per Minute |
| TOB | Torque on Bit |
| UCS | Unconfined Compressive Strength |
| WOB | Weight on Bit |
| Θ | Back rake angle |
| F_{cs} | Horizontal force on cutter |
| F_{cn} | Vertical force on cutter |
| ζ | Intrinsic specific energy |

| | |
|------------|--|
| ψ | Interfacial friction angle |
| d | Depth of cut |
| E | Drilling specific energy |
| S | Drilling strength |
| μ | Coefficient of friction |
| γ | Bit constant |
| l | Contact length |
| σ | Contact strength |
| F_c | Face cutter force |
| F_{ch} | Chamfer force |
| F_b | Back cutter force |
| σ_0 | Hydrostatic stress in crushed material |
| A_{ch} | Chamfer area |
| ω_d | Relief angle |
| α | Repression angle |
| ρ | Density |
| K_f | Bulk modulus |
| X_i | Position vector |
| R | Ball radius |
| g | Gravity |
| M | Mass |
| C | Damping Ratio |
| K | Spring Stiffness |

List of Table

| | |
|--|----|
| Table 1 Parameters of the PFC2D cutting environment | 18 |
| Table 2 Micro-properties of the rock created by Ledgerwood [15]..... | 20 |
| Table 3 Macro-properties of the rock created by Ledgerwood [15]..... | 21 |
| Table 4 Scheme for drill-off test with AE detection..... | 28 |
| Table 5 Inputs for monitoring acoustic emission..... | 29 |
| Table 6 Tests matrix of the pVARD tool rubber's O-rings | 64 |
| Table 7 Test matrix of the pVARD tool Springs | 64 |
| Table 8 The tests data result of the 6 rings springs..... | 69 |
| Table 9 Specifications of the 6" M716 PDC bit used in field work [3] | 76 |
| Table 10 The parameters of the field trials pVARD tool..... | 78 |

List of Figures

| | |
|---|----|
| Figure 1 Smith bit standard 6 inch Mi 711 PDC [2]..... | 7 |
| Figure 2 Blunt cutter force distribution in Detournay’s model [3]..... | 8 |
| Figure 3 Model of forces acting upon PDC cutter..... | 10 |
| Figure 4 PFC2D cutting environment [1]..... | 17 |
| Figure 11 Particle-size distribution from drilling with rigid compliance (upper), medium compliance (middle) and strong compliance setting (lower)..... | 34 |
| Figure 12 Particle-size distribution from different WOB..... | 36 |
| Figure 13 Particles obtained from drilling when WOB=516.65 Kg at strong compliance setting, whose size ranges from 850 to 2000 micron (upper) and from 420 to 590 micron (lower). | 37 |
| Figure 14 Single acoustic emission from rigid drilling when WOB= 202.20 Kg (upper) and spectrogram (lower)..... | 39 |
| Figure 15 Average event energy (upper) and event rate (number of triggered events per second, lower) from the trigger channel. | 39 |
| Figure 16 Average event energy versus ROP under three different complicate settings..... | 40 |
| Figure 17. Laboratory drilling system [39]..... | 45 |
| Figure 18 Single cutter DOC versus WOB for two drilling settings..... | 47 |
| Figure 19 MRR versus WOB for two drilling settings..... | 47 |
| Figure 20 MSE versus WOB for two drilling settings..... | 48 |
| Figure 21 Calibration process of PFC2D model..... | 49 |
| Figure 22 Illustration of PDC bit cutting process. | 49 |
| Figure 23 PVAR tool illustration and simplification. | 50 |

| | |
|---|----|
| Figure 24 Single cutter cutting process..... | 50 |
| Figure 25 Illustration of cutting area to measure the DOC and MRR..... | 51 |
| Figure 26 DOC versus WOB (simulation)..... | 52 |
| Figure 27 MRR versus WOB (simulation)..... | 52 |
| Figure 28 MSE versus WOB (simulation)..... | 52 |
| Figure 29 Y-position (mm) vs time (10-1sec) for rigid and pVARD, two simulations at WOB of 2500 N..... | 54 |
| Figure 30 Testing equipment set up with two parts of isolator and load is control by a hydraulic actuator..... | 59 |
| Figure 31 Recording computer and input/output national instruments analog (NI USB-6009)... | 60 |
| Figure 32 Rings of high-carbon steel Belleville dis springs are under tests..... | 61 |
| Figure 33 Work diagram: damping force VS displacement [47]..... | 61 |
| Figure 34 Effect of the raw record data (Left) and after filtering data (Right) on 15kN load, 2mm amplitude and 4.5Hz 6rings springs..... | 65 |
| Figure 35 Springs constant, the slope of the dashed line..... | 66 |
| Figure 36 Damper force (KN) versus velocity (mm/s)..... | 66 |
| Figure 37 Change in the spring constant (KN/mm) with frequency (Hz) and Amplitude (mm)... | 67 |
| Figure 38 Change in the damping coefficient (N.s/mm) with frequency and amplitude..... | 68 |
| Figure 39 Three rubber O-rings test data under 5mm amplitude with different frequency..... | 69 |
| Figure 40 Three rubber O-rings test data under 19Hz with different amplitude..... | 70 |
| Figure 41 A classical calculation graph and data of the rubber's damping..... | 71 |
| Figure 42 The field drilling site showing the pVARD tool (left), the PDC drill bit (center) and the SensorSub (right). [48]..... | 72 |

| | |
|---|----|
| Figure 43 Geological section of the field site constructed from the well drill cuttings analysis.[48]..... | 77 |
| Figure 44. The pVARD tool Bottom Hole Assembly (BHA) for field trials [34]..... | 79 |
| Figure 45 Drilling test results showing ROP for drilling in Red Shale with various pVARD and non p-VARD configurations. [34]..... | 79 |
| Figure 46(a). MRR, MSE and ROP for WOB of 40, 60, 80, and 100 kN and bottom-hole pressure ranging from 0 to 1000psi. MRR, MSE and ROP are in units of 10^{-3} m ³ /s, KJ/m ³ , and 10^{-2} m/s, respectively..... | 83 |
| Figure 46(b) MRR, MSE and ROP for WOB of 120 and 140 kN and bottom-hole pressure ranging from 0 to 1000psi. MRR, MSE and ROP are in units of 10^{-3} m ³ /s, KJ/m ³ , and 10^{-2} m/s, respectively..... | 84 |
| Figure 47 Comparison of MRR, MSE and ROP for rigid and pVARD drilling at all WOB and bottom-hole pressures. MRR, MSE and ROP are in units of 10^{-3} m ³ /s, KJ/m ³ , and 10^{-2} m/s, respectively..... | 85 |

Chapter 1 Introduction

1.1 Research Background

In this thesis, a polycrystalline diamond compact (PDC) bit is used as the primary bit for the simulation, experiment and study. PDC cutter was invented by General Electric (GE) in 1971. During the decades, this new cutter significantly increased the cutting performance and overtook the roller cone bits in the drilling bit market.

A large number of papers and people have been working on analysing on the interaction model of PDC (polycrystalline diamond compact) cutters and rock. A series of drilling experiments were carried out by using experimental equipment, in which load on cutters can be increased. Experiments were conducted with various loads, cutting areas, cutting speeds, back dip angles of PDC cutter and rock properties. The experimental results were usually analyzed with multiple nonlinear regression techniques and new cutter-rock interaction models were proposed many times. The previous research results show that the cutter area is the principal factor influencing the force of the cutters. The force of cutters increases with cutting area, back dip angle of PDC cutter, and rock drilling ability. It is a logarithmic relationship between the force of cutters and the cutting speed.

In 2008, a software tool was developed by Itasca Inc [1] to simulate the rock cutting. The simulation and its results can be used to study the mechanics and dynamic process during the cutting. In the cutting model built with PFC2D, there are three walls with zero friction created on the sides and bottom, and rock surrounded by the walls and a cutter. In the PFC2D rock cutting environment, rock is represented by particles. The cutter is set with fixed horizontal speeds, fixed

vertical speeds, and a fixed depth to be cut during the procedure. During the cutting, multiple parameters are monitored and recorded, including velocity, force, depth and energy.

1.2 Research Purpose and Objectives

In this research, the author investigates the comparison between experiment and numerical simulation towards new pVARD tool. Setting up the numerical simulation for the tool can help us to model the different hard conditions, such as high bottom-hole pressure (BHP), high flow rate, extremely high weight on bit (WOB) and different rocks, which is difficult or even impossible to implement in the real drilling.

Meanwhile, through the analysis of passive VARD tool performance, such as Rate of Penetration (ROP), cuttings from the field trip and laboratory, we could clearly found that the pVARD tool help to develop the rate of penetration and increase the drill efficiency. Especially, under specific Bottom-Hole Pressure (BHP), the pVARD tool in the field work drilling and simulation indicating a dramatic 3 times to 4 times increased performance increase compared to conventional rigid rotary drilling.

1.3 Significance Process of Research

Comparing the different drilling methods and drilling tools, it is important to research on bit-rock interaction of drilling tools by using new method. And then, our ADL group's new drilling tool which named passive Vibration Assisted Rotational Drilling (pVARD) tools were created, it is necessary to study on potential impacts on penetration rate with numerical simulation and experimental validation. So, meanwhile, our ADL group brought in DEM simulation method which is a novel prediction method of ROP for PDC bit in drilling.

In short, many drilling tests were finished, not only in the Drilling Technology Laboratory (DTL) in which load on cutters can be increased. Experiments were conducted with various loads, cutting area, cutting speed, back dip angle of PDC cutter and rock properties. The experimental results were analyzed with multiple nonlinear regression technique and a new cutter and rock interaction model was proposed. The results show that the cutter area is the principal factor influencing the force of cutters. Interaction model of PDC cutter and rock are set up by DEM model, combining with previous group members' PFC model and bit rock interaction model, a new model which adds spring stiffness and damping coefficient and could completely simulate the new passive vibration tool was set up by the author.

The force of cutters increases with cutting area, back dip angle of PDC cutter and rock drill ability. It is a logarithmic relationship between the force of cutters and cutting speed.

During these two years, the author has two major areas, one is the SWD Seismic While Drilling and another is PFC2D simulation for pVARD drilling. At the beginning of the research, all the group members joined a VARD tool field trial. It finished all the VARD performance on field drill off tests, and at the same time obtained SWD data and sensor-sub data for different bits such as PDC, RC and Hammer bit.

Secondly, the sensorsub data is analyzed. 1) Extract specific sensorsub data for drilling sections to obtain downhole bit vibration including axial, lateral and torsional vibrations. 2) Correlate vibration data with time, WOB, ROP, and RPM. 3) FFT analysis. It be done for each section to check the vibration spectrum which helps to describe bit vibration situation and SWD data.

Thirdly, the lab pVARD tool drill off test and SWD test. In this part: 1) we finished non-vibration drill off tests with seismic detection; 2) cuttings collection and heating which is ready for microscopic analysis; 3) finished pVARD vibration drill off tests with seismic detection: mix, double strong, double weak and single strong, single weak strength. 4) cuttings analysis under microscope, simply one by one starting from cutting sample shaking machine.

In the second main research area: PFC2D simulation. In this short two years, the author learned to use PFC2D simulation in single cutter bit model and to write code. All the parameters are calibrated and corrected. The simulation program, code and all the parameters match the lab data. Test the damping coefficient and spring stiffness of the field and lab rubbers and springs, and then input all the field work data into the PFC simulation and write a journal draft about how to test that damping and spring. Run all of the real data in the simulation to find the boundary if the PWARD tool. Damping coefficient and spring stiffness, three ball contact model have been applied. Dampening tool equation is being discussed and adjusted now. Calculated the MRR, MSE and ROP data from lab are analyzed for the simulation result and published the paper.

In conclusion, in this part, all the MSE, torque and other data is compared with lab and simulation. After hard work on cutting analysis, five different strength data and good FFT amplitude results were got, and this ideal result matched field work result. The seismic data of three wells in field work is processed using VASTA, and it is clearly identified as S-wave and P-wave. Seismic data is needed to be matched the data of sensorsub. Meanwhile, RC and PDC data was analysed section by section. In addition, laboratory drill-off tests with acoustic emission detection and lab scale drill-off tests with VARD and without VARD are conducted. Cutting size was analysed for interpreting improved drilling performance. Acoustic emission energy for

explaining improved drilling performance. The author also successfully correlated the improvement of drilling performance, cutting analysis, and acoustic emission.

Chapter 2 Literature Review

2.1 Penetration Mechanism of PDC bits

2.1.1 Research and development of polycrystalline diamond compacts (PDC)

Polycrystalline diamond compact (PDC) is composed of a polycrystalline diamond layer and a hard alloy layer. This new material not only has high hardness and high wearing resistance, but also has the advantage of strong shock resistance. Integrating the above advantages, PDC has been widely used in earth drilling, cutting of various materials such as non-ferrous metals and their alloy, hard metal alloys, graphite, plastics, rubber, and ceramics. It is contained with polycrystalline diamond sintered from diamond powder. Thus, it can be used as separate cutting unit. Since the development of PDC bits and single cutters, they both have been widely applied in drilling engineering. In the process of practical drilling, the wear of broken tools is the main problem in rock-breaking, so the operating performance of the bit directly influences the well drilling quality, efficiency and cost. Especially, when the rocks compressive strength of the layers is over 150Mpa, the mechanical breaking of rocks in the drilling process is very difficult. In this case the drilling engineers must strengthen the breaking-rock tools through changing the shape and material of the bits. To enhance the working performance of the tool, they also need to research the mechanism of the rock breaking. PDC bit drilling takes the hard rock properties, formation characteristics, outer load conditions and the structure of artificial bit cutting rock into consideration. It will fundamentally and comprehensively address the root problem of the bit rock interaction.

(152.4 mm) ID:64816A0201
ER:25536

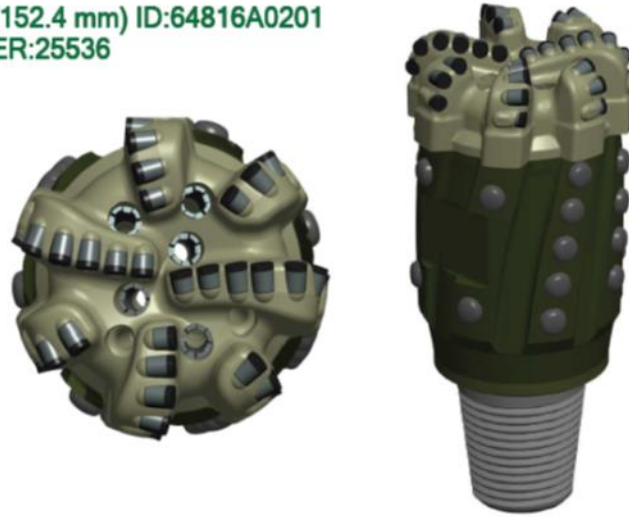


Figure 1 Smith bit standard 6 inch Mi 711 PDC [2]

This PDC bit (Figure 1) have three main strengths: first, minimize vibration to increase stability and superior wear resistance; second, reduce cutter damage for maximum drilling length; and third, retain sharp cutting edges for higher ROP.

2.1.2 The role of single PDC cutters in rock stress analysis

The mechanical property and drill-ability of rocks are the basic parameters available for analyzing and evaluating the anti-fracture and drilling resistance of rocks. In the production process of a PDC bit, the PDC needs to be inserted into the drill bit, so when the PDC bit is in the drilling process, its force direction is inclined to press in and break the rock. PDC cutter only is effected by the normal force and the vertical pressure make the half body space of the cutter into elastic rock. The radius of the cylinder is set to R . D is the pressure depth of the cylinder. Θ is the cutting angle, and it also is the angle of the elastomer surface with the PDC axial. The mechanism of the PDC bit cutters being pressed into the rock is complex, because the cutters geometrical shape on the bit is difficult to describe. In order to simplify the calculation, the

force on the bit could be described in several parts. According to Detournay's model [3], one part is normal force on the rock and another is the shear force on the bit bottom and rock. (Figure 2)

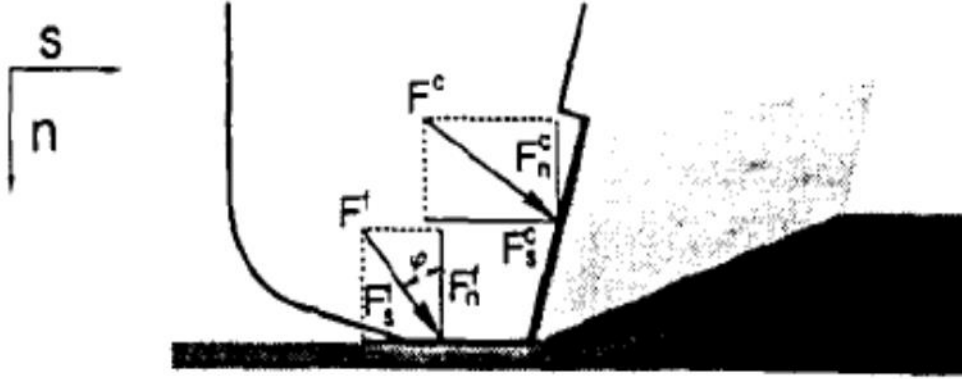


Figure 2 Blunt cutter force distribution in Detournay's model [3]

Where, the normal and shear forces, Weight on Bit (WOB) and Torque on Bit (TOB) can be computed respectively:

$$F_n = F_n^c + F_n^f \quad (2.1)$$

$$F_s = F_s^c + F_s^f \quad (2.2)$$

$$W = W^c + W^f \quad (2.3)$$

$$T = T^c + T^f \quad (2.4)$$

The ideal cutter equations for the cutting component of the weight on bit and the torque can be expressed as follows:

$$T^c = \epsilon d \quad (2.5)$$

$$W^c = \zeta \epsilon d \quad (2.6)$$

Where, d is the depth of cut (DOC) per revolution.

Moreover, the researchers also established the formula of Drilling Specific Energy and Drilling Strength as:

$$E = T/d \quad (2.7)$$

And

$$S = W/d \quad (2.8)$$

Detournay suggested a linear relationship between the specific energy and the drilling strength:

$$E = E_0 + \mu\gamma S \quad (2.9)$$

In addition, after the Detournay model [4], Gerbaud et al. [5] created a new model in 2006 which takes both the forces acting on the back of the cutter and the forces acting on the chamfer into consider:

$$F = F^c + F^{ch} + F^b \quad (2.10)$$

The total forces on the cutter are consist three components of force: forces acting on the cutter face (F^c), forces acting on the chamfer face (F^{ch}), and forces acting on the back of the cutter (F^b) (Figure 3).

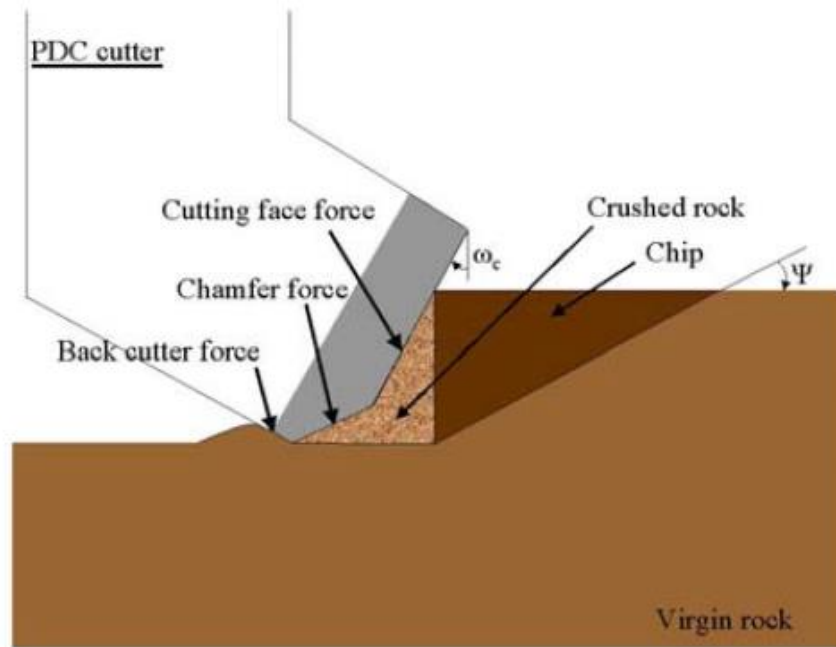


Figure 3 Model of forces acting upon PDC cutter [4]

Based on previous studies, the Ledgerwood research group [6] conducted a series of experiments to investigate the effect of crushed particles beneath the cutter on drilling performance. It is concluded that these particles, once they are under hydrostatic pressure, will have very high strength, and even the lowest strength is close to that of the virgin rock. Additionally, this study [6] not only focuses on the drill-ability of the different rocks under hydrostatic pressure, but also proves that inelastic properties of rock have more effect on the rate of penetration (ROP) than elastic properties[7].

2.1.3 Analysis of the rock cutting mechanism

When analyzing the rock cutting mechanism, there are several conditions to be considered together, including external load on the tool, the properties of the tool itself as well as characteristics of the rock. Hence, not only the cutting effect needs to be studied, but also the

trend and stress state before and after cutting. Mechanical properties are the basic characteristic of rocks, like the relationship of stress and strain is the basic factor to understand rock. Uniaxial compressive strength is the ratio of axial pressure and area when the rock is crushed only by axial pressure. The expression is as follows.

$$\sigma_c = \frac{F_c}{A} \quad (2.11)$$

The rock stiffness means the ability of local deformation or breaking under the pressure of concentrated load, which is expressed by pressure over area.

$$\sigma_K = \frac{P}{A} \quad (2.12)$$

Plasticity describes the process of rock undergoing non-reversible changes of shape, which has significant influence on drilling and breaking effects. In the drilling process, a PDC bit can break different rock formations from soft to hard strength level. In general, PDC bits break the rock primarily by cutting or shearing, and only secondarily by crushing. The actual breaking process is depending on different rock formation types.

2.2 PVAR D Drilling Tools

Recently, a passive VARD tool was designed by DTL to increase the rate of penetration (ROP), increase drilling efficiency, and reduce the energy consumption per volume of penetrated rock. In the past two years, several papers were published related to this tool and many laboratory tests and a field trial all proved that the pVAR D is useful for improving drilling performance. When the bottom-hole pressure increases, the ROP decreases. The use of the pVAR D tool helps to overcome the increase in pressure, thus increasing drilling efficiency,

reducing drill time and drill costs. The springs within the axial compliant section provide axial compliance. The VARD tool provides an optimal level of axial displacement at the drill bit while transmitting the full penetration rate. See the appendix for the detailed drawings of the VARD tool, as well as included the calibrations and tests that were conducted in the lab with the lab scale VARD tool before the field trials.

2.3 Distinct Element Method (DEM)

The Distinct Element Method (DEM), usually named discrete element method, is one of the numerical methods for computing the motions and effects of a large number of small particles [8]. Though DEM is very closely related to molecular dynamics, the method is generally distinguished by its inclusion of rotational degrees-of-freedom as well as stable contact and often complicated geometries (including polyhedral). Nowadays, DEM is becoming widely accepted as an effective method of addressing engineering problems in granular and discontinuous materials, especially in granular flows, powder mechanics, and rock mechanics. Recently, the method was expanded into the Extended Distinct Element Method taking thermodynamics and coupling to CFD and FEM into account.

Distinct element methods are computationally intensive, which limits either the length of a simulation or the number of particles observed. Several DEM codes, as well as molecular dynamics codes, take advantage of parallel processing capabilities (shared or distributed systems) to scale up the number of particles or the length of the simulation. An alternative to operating all particles separately is to average the physics across many particles and thereby regard the material as a continuum. In the case of solid-like granular behaviour formed in soil mechanics, the continuum approach usually treats the material as elastic or elastic-plastic and models it with

the finite element method or a mesh free method. In the case of liquid-like or gas-like granular flow, the continuum approach may treat the material as a fluid and use computational fluid dynamics. Drawbacks to the homogenization of the granular scale physics, however, are well-documented and should be considered carefully before attempting to use a continuum approach.

The DEM method can be applied in many research areas, such as liquids and solutions dynamics, bulk materials in storage silos, granular matter, powders and blocky or jointed rock masses. In drilling and mining engineering research, we use it in rock cutter interaction simulations. The previous research and past DEM modelling work that were done by other graduate students in the Drilling Technology Laboratory (DTL), includes Babak Akbari[9], Hossein Khorshidian[10], Mohammad Mozaffari[11] and Yousef Gharibiyamchi[12].

Babak Akbari set up the DEM model to simulate the single cutter of the Polycrystalline Diamond Compact bit-rock interaction in 2011. In his research, a physical model of a single PDC cutter is developed, with the ability of changing the parameters. This model is the first time in our DTL group based on the Distinct Element Method, and it is used to simulate the cutter's interacting with rock surface. Important parameters such as force and velocity can be changed to reach different results, which will reflect the change on drilling performance.

Based on Akbari's research, the thesis of Khorshidian, Hossein [10] added the influence of borehole pressure and bit hydraulics on the performance of a drill bit.

In addition, Mohammad Mozaffari[11] developed the simulation and analysis a characterization of Portland Cement-based synthetic rock materials. Focusing on rock properties, Mohammad tests three kind of concrete, which are strong medium and weak material. Also, he did correction use the PFC2D model to find the effect of gap on Young's Modulus, Poisson's

ratio, friction angle vs CCS, failure behaviour, tensile strength, minimum Particle size and the resolution of all of them.

Recently, Gharibiyamchi[12] used DEM to simulate the action of the real AGT and the hydropulse tool. After adding the different simulation scenario in the AGT and the hydropulse tool, he compared the different result of the simulation with and without shock tool. His simulation results showed significant increase in drilling performance when the AGT and hydropulse tool was applied. In addition, he found that the performance of the AGT was better than that of the hydropulse tool. Therefore, from here our DTL group began to simulate the real drilling tool, not only just bit or cutters.

Vibrations, Weight on Bit (WOB), Depth of Cut (DOC) and Rate of Penetration (ROP) have consistently been four primary concerns when designing the DEM simulation model of a pVARD tool. How to consider these key points and integrate them into the DEM simulation are the problems to be addressed in this thesis.

2.4 Cutter-Rock interaction

Based on previous literature and research, in order to study the mechanical characteristics of the cutter during the rock cutting process and to predict the average peak force reaction on the cutter, a numerical model of rock cutting is established based on fracture mechanics and discrete element theory. The rock cutting process directly affects the mechanical action of the stability of the drill bit. The accurately predicted of average peak force on the cutter, the drill bit selection and design as well as rock cutter interaction structure design are all important factors for study. According to the numerous studies in the past, Ranman[13] analysis the force of the rock cutting process. He point out that the peak force on the cutter is three times bigger than the average force. After that, Copur etal [14] conducted many cutting experiments on a variety of

rock samples. In addition, Bilgin et al [15] took a rock and cutter interaction study on 22 different kinds of rock samples. And then, he provided a relationship between the force on the cutter and compressive strength of rock, tensile strength as well as dynamic and static elastic modulus. Evans[16]、Roxborough and Liu[17] and Goktan[18] based on the theory of maximum tensile stress built a force of cutter model in cutter rock interaction process. They argued that the rock breaking is mainly dependent on the tensile stress of the cutter breaking into the rock. The module is mainly relative to the mechanical properties of rock and the role of the cutter parameters. It is widely used in rock-breaking mechanism research all over the world. The process of the rock reaction on the cutter is simulated and investigated.

The reaction forces on the cutter are obtained with different rock mechanical characteristics and impacted the conditions of the cutter. The results show that the impacting velocity within a certain range has less effect on the peck cutting force and the variation of reaction force is unanimous to rock volume changes with stepwise decreasing. The relationship of average peak force reaction on the cutter obtained from simulations, experiments and theoretical models was investigated with the linear regression analysis. From this thesis following chapters results show that the linear correlation coefficients between numerical results and the results of experiments and Goktan's[18] theory are in agreement with each other. It is confirmed that this numerical model is feasible to simulate the rock cutting process.

Chapter 3 Distinct Element Method (DEM)

modeling of the Cutter Parameters

3.1 Brief Description of PFC2D Software

The Particle Flow Code in 2 Dimensions (PFC2D), which was created by Itasca International, Inc. This company set up the PFC numerical modeling in micromechanics via Particle Methods and rock-cutting Procedures. The PFC codes are used to simulate rock cutting to learn more about drilling mechanics[1]. PFC models allow one to define a cutter (as a set of walls), and move this cutter at a specified velocity and depth of cut across a synthetic rock, while monitoring forces on the cutter and damage in the rock. In a real borehole, drilling mud produces a pressure that acts on the rock surface, and this pressure greatly increases the energy requirements of drilling, it effectively strengthens the rock.

3.1.1 PFC2D Rock-Cutting Environment

A parameterized rock-cutting environment for PFC2D is described in this section. According to the Itasca company, this environment supports the creation of a bonded-particle model of the rock, specification of a cutter (represented as PFC walls), the pressure to be applied to the rock surface, the movement of the cutter at a fixed depth of cut. All of the rock can be reflected in PFC2D particles. The particle-size refinement procedure in the PFC Fishtank can be used to construct graded particle assemblies with smaller particles in the cutting region and larger particles in the far-field region. The PFC2D cutting environment is shown in Figure 4, and

the parameters are listed in Table 1. The specimen is rectangular (H , W) and confined by three frictionless walls on the bottom, from the left to the right sides. The cutter consists of a single wall of two segments (both of length l) that are perpendicular to one another with a back-rake angle of θ . The confining pressure is P . The cutter is moved horizontally across the rock at a velocity V and at a depth of cut D .

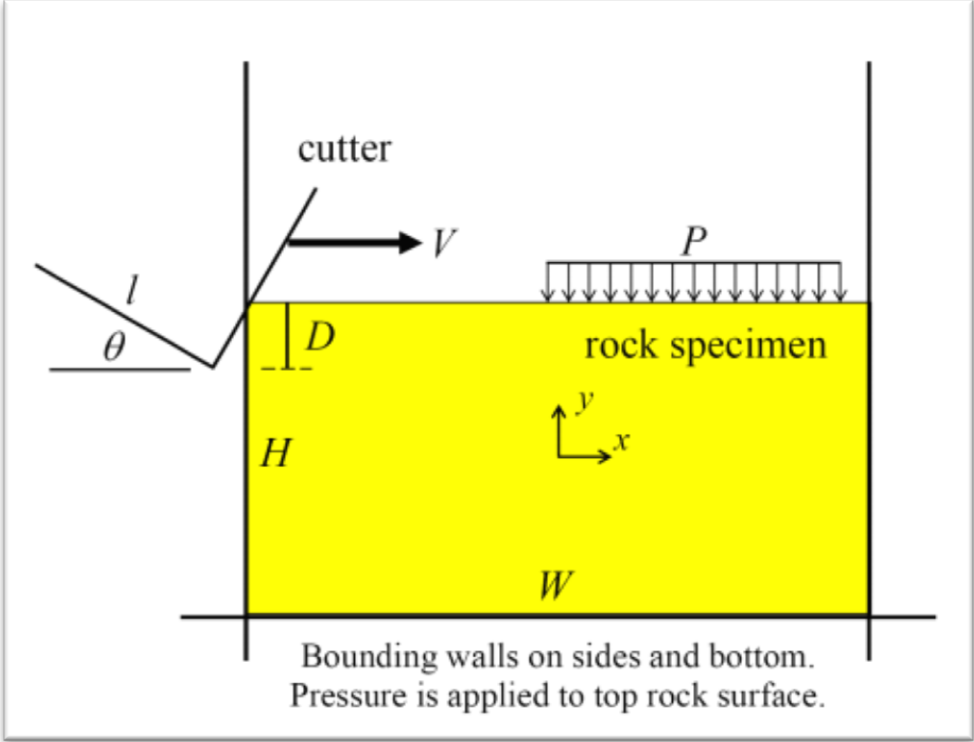


Figure 4 PFC2D cutting environment [1]

Table 1 Parameters of the PFC2D cutting environment [1]

| Symbol | FISH Symbol | FISH Type | Default | Name |
|----------|-------------|-----------|---------|--|
| H | mv_H | FLT | NA | specimen height |
| W | mv_W | FLT | NA | specimen width |
| l | ct_length | FLT | NA | cutter length |
| θ | ct_rake | FLT | NA | cutter back-rake angle ($0 \leq \theta < 90^\circ$) |
| V | ct_speed | FLT | NA | cutter velocity |
| P | ct_press | FLT | NA | confining pressure |
| D | ct_depth | FLT | NA | depth of cut ($D \geq 0$) |
| G_f | cs_usegap | BOOL | 0 | use-gap flag; if set, then specify $\{G_a, G\}$ |
| G_a | cs_gapabs | BOOL | 0 | use absolute magnitude flag |
| G | cs_gap | FLT | 0.0 | gap value |

According to the manual of PFC2D software modeling which was published by Itasca [1], this tool uses FISH as its main programming language. PFC Fishtank is used as a consistent set of FISH functions to extend the range of modeling. With this programming language (FISH) and efficient modeling tool (PFC2D), a user like the DTL group could use it to simulate the drilling process. When creating and building the cutting environment, all the relevant parameters need to be input, including cutter-length, back-rake angle, cutter's velocity and specimen dimensions. PFC2D could then simulate the drilling process on instantly and consistently. Meanwhile, the PFC gives details and values on every parameter that could monitor the process of the bit-rock interaction. In addition, drilling mud should also be taken into consideration, because the mud is viscous liquid which cannot sustain shear stress, it can be regarded as pressure on the rock surface.

In order to load the pressure on the rock, several procedures need to be completed. The first step is to set up the tool which the user needs to simulate on the cutter, and then set up the cutter. The second step is build up the simulate rock and the wall of the simulation boundaries should be created at the same time. As such, the load could input from the top of the tool to the cutter and across crushed rock particles that form under the cutter and finally transmits normal load to the rock material and average effect on walls or outer boundaries of the system. The PFC2D pressure-application procedure is complex and has a special file named fist\2d\ch.fis and fist\2d\ct.fis. The command of this code file to connected chains of particles spanning and transferred the pressure from the cutter face to the both sides of the wall.

3.2 Simulation of drilling rock, microscopic and macroscopic Properties

To simulate the real drilling rocks, there are many problems to be considered. It started from the Itasca company fundamental rock testing to the Ledgerwood [19] research, and then Babak Akbari research on the PDC bit-rock interaction [9], after the Hossein and Mohammad rock material test model, till now, the mature rock simulation system have formed. It was set up by DTL group step by step. Simulating the formation rock under the DEM modeling environment is a complicated process. Through the efforts of several generations, the rock simulation has experienced several developing periods.

According to the Ledgerwood [19], to simulate a rock is to establish balance in density, Young's modulus, Poisson ratio, UCS and friction angle. No matter the real rock test or simulate rock all need to be tested for these parameters to be calibrated for use. For the simulations of the pVARD tool, the Ledgerwood rock simulation parameters that were used to calibrated and

simplify the data process. Ledgerwood conducted many triaxle tests simulation in order to correct the rock he simulated to match with the real rock conditions. The micro-properties of the rock and the Macro-properties of the rock simulated by Ledgerwood's were demonstrated separately in Table 2 and Table 3. The following idea of Vajdova et al [20] and Wong et al [21] show that most rocks transit from shear localization to shear-enhanced compaction with increasing confining pressures, Ledgerwood used this idea in calibrating his simulation rock. In the shear localization mode, large elastic wedges of material slide past each other along the combined cracks along diagonal shear planes. In shear-enhanced compaction mode, most of the rock volume is failed [19]. After conducting a series of triaxial tests to confirm these phenomena by PFC2D, he observed the exact patterns that in real life. Due to this thesis study on the efficient of the pVARD drilling tool and use most of the medium strength rocks and concrete samples ($30 \text{ MPa} < \text{UCS} < 80 \text{ MPa}$), this rock is an ideal choice for drilling simulation of the tool in this case. Meanwhile, based on the Ledgerwood data analysis, the DTL group members corrected the rock generation code for PFC2D FISH language and could be appropriate for PFC2D environment.

Table 2 Micro-properties of the rock created by Ledgerwood [19]

| Property | Magnitude |
|--|---------------------------------|
| Ratio of Maximum to Minimum Ball size | 1.8 |
| Parallel Bond Shear Strength | $44 \times 10^6 \text{ Pa}$ |
| Parallel Bond Normal Strength | $44 \times 10^6 \text{ Pa}$ |
| Minimum Ball Radius | $0.35 \times 10^{-3} \text{ m}$ |
| Ball and Bond Elastic Modulus | $40 \times 10^9 \text{ Pa}$ |

| | |
|------------------------------------|-----|
| Ratio of Normal to Shear Stiffness | 2.5 |
| Ball-ball and Ball-wall Friction | 0.5 |

Table 3 Macro-properties of the rock created by Ledgerwood [19]

| Property | Magnitude |
|---------------------------------------|------------------------|
| Density | 2650 kg/m ³ |
| Porosity | 18 % |
| Normal Damping Ratio | 0.2 |
| Shear Damping Ratio | 0.2 |
| Local Damping Ratio | 0.5 |
| Unconfined Compressive Strength (UCS) | 55 Mpa |
| Young Modulus | 40 Gpa |

In addition, for the different drilling rock, microscopic and macroscopic properties, Mozaffari[22] in DTL conducted a series of tests and modified them in the PFC. In his research, not only simulate the loose sand stone but also have the UCS and CCS tests for different strength of rocks. For example, it provided different strength of concrete samples parameters, such as high strength, medium strength and low strength.

3.3 Simulating on Single Cutter Penetration Considerations and Input Parameters

For the single cutter penetration we set up two main kinds of different simulation cutters. One is simulate like the Lab scale PDC cutter (Fig.3) which is two main cutters and when simulation this cutter half weight on bit will on it. Another field work scale cutters of PDC bit is mentioned in the chapter two and WOB also divided by cutters number on one single cutter. The single cutter all built up like a corner of the wall which was consisted of 00balls to simulate it and the tool simulation and the load are all built up based on this cutter's simulation

It is depends on different scales of the experiments the DTL group did, there are different input parameters we should take into consideration in the simulation. The lab scale simulation matrix will be demonstrated in the Chapter 4 and the field work scale simulation will be shown in the Chapter5. Actually, there are three significant characteristics should be focused on: first, the vertical force on the cutter; second, the rotary speed; third, the bottom-hole drilling fluid pressure; forth, the rock types and density; the last is the cleaning efficiency.

Due to the real condition of the pVARD tool, the vertical force on cutter is always the weight on bit (WOB) add the forces which generated by the pVARD tool (spring force and the damping force). In addition, because this is the PFC2D simulation, as the normal condition [22], the constant Revolution per Minute (RPM) of the bit was changed to suit for the PFC simulation, rotary speed was usually set up on 75RPM [12]. The calculation process will be attached in appendices.

Meanwhile, the bottom-hole drilling fluid pressure for the lab drill off test is under the standard atmosphere, for the field work is different between 0psi to 1000psi. For the rock types

and density, we usually simulate as the medium strength concrete and similar with the red shale [23].

Finally, the cleaning efficiency should be another important consideration. Development of the previous studied showed that the most effective cleaning condition in the PFC2D drilling environment is 1. Due to the one ball in the simulation is contacted with other 4 balls, and the code and model is set up in a way that it provide a cleaning efficiency of 1, 2 and 3 to the cutting process. Cleaning efficiency of 1 means that any ball that has maintain only one contact and three broken contacts is deleted from the cleaning zone. In addition, the cleaning efficiency of 2 shows that any ball that has two contacts or lower (more than two balls are broken) is deleted from the cleaning zone. A cleaning efficiency of 3 stands for a situation in which any ball that has three contacts or lower is deleted from the cleaning zone, which means if one contact breaks between two balls, both of them will be deleted. Since cleaning efficiency level 3 delete approximately half of the balls in the system, it is too cleaning to be eliminated first. Combined precious research simulation model of Mozaffari[11] and Gharibiyamchi[12], and also compared the cleaning efficiency of 1 and 2, after some of the simulations run, it come to a result that cleaning efficiencies of 1 is the best and it closest to reality. Therefore, level 1 of the cleaning efficiency was selected for the simulations of the rigid condition and the pVARD tools both in the field work and the lab.

Chapter 4 Investigated Lab PVAR D Tools and Operational Mechanism with Discrete Element Method (DEM) Modeling of the Lab Scale Tool

This chapter is the paper “Micro-Seismic Monitoring of PDC bit drilling performance during Vibration Assisted Rotary Drilling” authored by Yingjian Xiao, Jinghan Zhong, Charles Hurich, and Stephen Butt, and was published in the Proceedings of the 49th US Rock Mechanics/Geo-Mechanics Symposium, San Francisco, USA in June 2015. The MEng candidate was involved with the planning and execution of the drilling experiments, the experimental data analysis, and the writing of the paper. Lab Test Equipment: Drilling Rig (Small Scale Drilling System) is used in the test. A laboratory scale drill rig was set up to conduct the PVAR D tool drill test. This Small Scale Drilling System (SDS) constitutes of many main systems, such as the rotary system, the loading system, the circulation system, the compliance (VAR D tools) system, and the data acquisition system.

Abstract

This study is an evaluation of the feasibility of real-time drilling performance monitoring using a near-bit AE detection tool in drilling with PDC drag bits under laboratory conditions to

investigate an improved drilling performance with a new Vibration Assisted Rotational Drilling tool. This paper focuses on calibrating the micro-seismic response to rock failure mechanisms, improved Rate of Penetration (ROP) and cutting particle-size distribution. Concrete cylinders with comparable properties to natural rock were fabricated in the laboratory. Drill-Off Tests (DOT) were conducted under rigid and compliant drilling with a two-cutter PDC bit. Simultaneously, micro-crack Acoustic Emissions (AE) from the bit-rock interaction process were monitored by four symmetrically mounted Non-Destructive Testing (NDT) sensors. The fracture characteristics were investigated by analyzing acoustic events in terms of event occurrence rate, and average event energy. Analysis from the DOT indicates that some factors are correlated with improved drilling performance, including particle-size distribution, vibration compliance setting and acoustic emission. A stronger vibration compliance setting increases ROP by increasing cutting depth per revolution and bigger cuttings are generated. Higher average event energy corresponds to bigger cracking when cracking event rate increases. All of this has contributed to our understanding of the mechanisms of improved drilling performance.

4.1 Introduction

One of the major problems for field drilling engineers is how to drill to target formations fast and safely. In drilling subsurface formations a vertical oscillation generator was found to increase penetration rate [24] and this early stage of oscillation vibrator drilling was called Resonant Sonic Drilling. After that, both surface and offshore mechanical vibrator were introduced [25]. Vertical vibration applied to a bit leads to fluctuations in WOB which interact with rock. A new vibration tool developed in the Advanced Drilling Laboratory (ADL) at Memorial University was tested for improving ROP [26, 27, and 28]. Laboratory tests have

shown that controlled amplitude and frequencies of vibration are available from this vibration tool and the effect of vibration on drilling efficiency and penetration rate was investigated.

Micro seismic events, or acoustic emission (AE), are the elastic waves produced when rock undergoes internal change, such as micro crack initialization and propagation. In non-destructive testing (NDT), piezoelectric transducers are commonly employed in detecting and monitoring micro crack propagation. As an alternative way to ‘see’ micro crack initiation and propagation, AE detection has been applied in triaxial compression tests to monitor the whole deformation process [29]. Some AE parameters such as dominant frequency, event energy and cumulative emission counts are related to the different deformation stages. Numerical simulation with PFC2d models has been used to simulate UCS tests to predict rock failure [30, 31]. In this PFC model, hit number is scaled by counting crack number under tri-axial compression tests. AE detection is commonly used in hydraulic fracturing (HF) researches. Fluids has been injected at high pressure into cylindrical rock to simulate hydraulic fracturing with AE detection of crack initiation and propagation [32].

4.2 Experimental Setup

Monitoring acoustic emission while drilling was based on drill-off tests along with cutting collection. A small drilling simulator was applied in this experiment which was used before by other researchers of ADG [33]. Modification of the drilling system to facilitate was measuring acoustic emissions and cutting collection. The drilling system is shown in Figure 5.

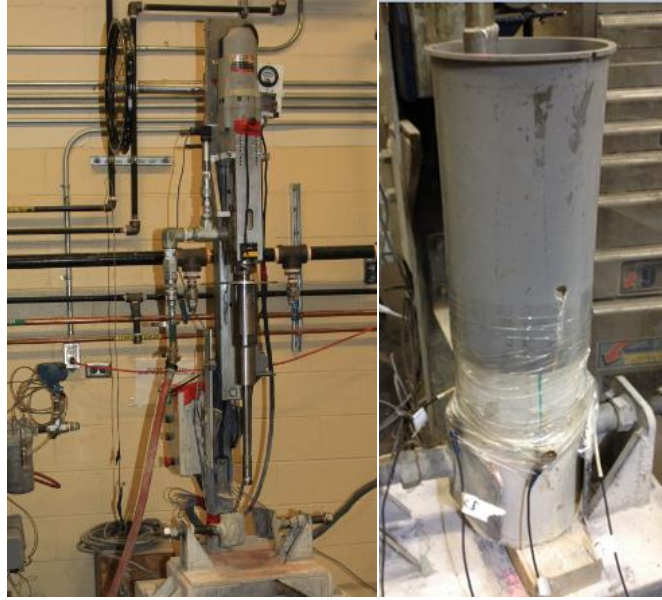


Figure 5 Generic view of small drilling simulator (left) and cutting collection and acoustic emission setup (right)

4.2.1 Test Materials

The drill-off tests were conducted on one synthetic concrete with the un-confined compression strength (UCS) of about 40 MPa. This concrete was made of aggregate, cement, and water with the mass ratio of 4:1:0.6. The dimensions of the concrete cylinders were 4 inch outer diameter by 6 inch height. One test sample was required for each variation in drilling parameters. Before the test, portions of the cylindrical surfaces are ground to flat for attachment of acoustic emission sensors.

4.2.2 Small Drilling Simulator

The atmospheric drilling is simulated by one small drilling simulator. WOB is applied by a mass suspended on a wheel and torque by motor acting through gears. There are two settings for the rotary speed, 300 rpm and 600 rpm. In the paper, only tests at 300 rpm are reported. A constant flow rate of tap water is used for bottom-hole cleaning.

A two-cutter PDC bit with an outer diameter of 35 mm was used. A laser sensor was attached on the moving part of the rig which can measure the bit vibration within a working amplitude range of 20 mm.

A p-VARD vibration tool is applied on the top of drill string with two compliance settings labeled medium and strong compliance [34]. The compliant section converts bit vibration into the axial displacement. And the damping part absorbs harmful vibrations are aim at preventing the drill-string from damage. In this paper, three different settings of compliance are utilized. The proposed scheme for compliance setting of drill-off test is listed in Table 4.

Table 4 Scheme for drill-off test with AE detection

| Compliance setting | Rated rotary speed (rpm) | Flow rate (US gpm) | Depth for each run (mm) |
|--------------------|--------------------------|--------------------|-------------------------|
| Rigid | 300 | 0.68 | ~15 |
| Medium | 300 | 0.68 | ~15 |
| Strong | 300 | 0.68 | ~15 |

4.2.3 Monitoring Acoustic Emission

Four P-wave sensors were placed symmetrically around the cylindrical concrete samples. Shear wave couplant was put between sensor and concrete surfaces to optimize signal transmission. The central frequency of p-wave sensors was 1.14 MHz with working bandwidth from 0.65 to 1.63 MHz at 6dB attenuation. From the frequency spectrum calibration report, the wide range of bandwidth guarantees reliable signals obtained from concrete even if the dominant frequency of signal is not located exactly inside the best working bandwidth. Four PAC 2/4/6 preamplifiers were utilized and the gain which was selected as 20dB is applied in the laboratory drilling tests. Four customized power supply adapters are connected to these preamplifiers with

output voltage of 20 volt. The DAQ system was comprised of GaGe CompuScope 8280 eight-channel board and built-in DAQ software. The on-board memory of 128 MB allows saving up to 250 triggered events per channel to the computer disk. The trigger sensor was always put closest to the drilling source.

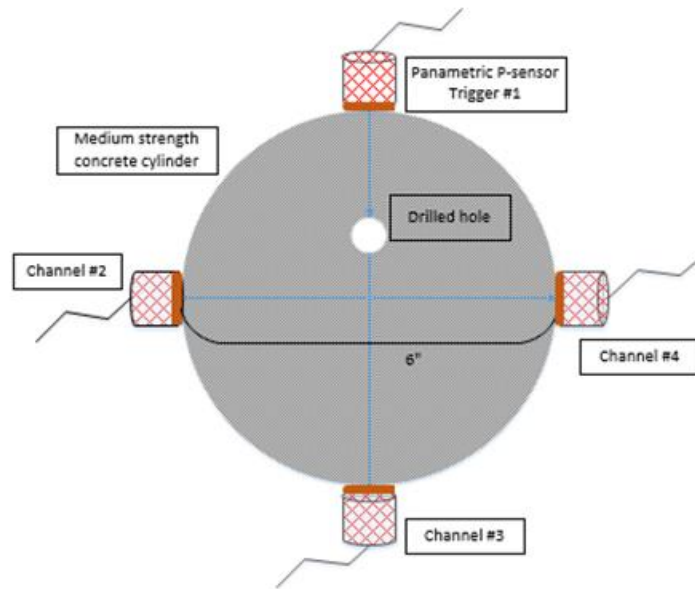


Figure 6 Top view of p-sensors distribution around synthetic concrete cylinder

The overall working flow chart for monitoring acoustic emissions is displayed in Figure 6. All signals are automatically saved to computer disk when all settings are set well before each run of test. All settings for acoustic emissions detection are displayed in Table 5.

Table 5 Inputs for monitoring acoustic emission

| Sampling frequency | P-wave sensors # | Gain | Peak-peak input | Trigger level |
|--------------------|------------------|-------|-----------------|---------------|
| 10 MHz | 4 | 20 dB | 10 V | 0.05 V |

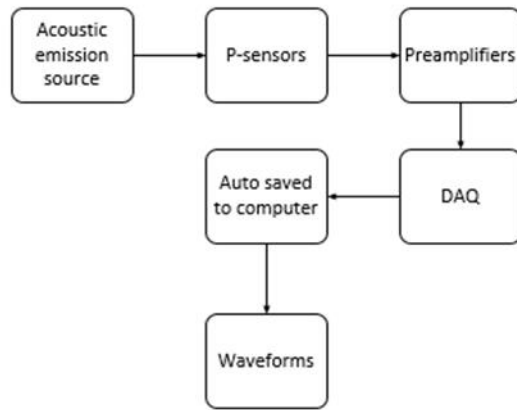


Figure 7 Flow chart for monitoring acoustic emissions

4.2.4 Cutting Analysis Overview

For each run of drill-off test, all cuttings were collected from the fluid flow outlet. The concrete top surface was sufficiently cleaned for next run of test. Following ASTM standard D6913–04 [35] and cutting analysis procedure from researchers in DTL [23], collected cuttings were fully dried and different range of cutting size was analyzed with sieves with apertures 2000, 850, 630, 590, 420, 300, 160, 75, and 37 micron. The smallest size of cutting was assumed to be 10 micron which was convenient for calculating particle-size distribution.

For smaller size of cuttings below 37 micron, no more sieve analysis was done due to the small amount of mass. Furthermore, cutting size analysis whose sizes were smaller than 37 micron could be done with hydrometers [36].

4.3 Results

During the drill-off tests, drilling related and acoustic emission data were monitored and saved automatically. Drilling performance parameters included penetration depth, duration, WOB, flow rate, bit vibration magnitude. Synchronized acoustic emission data obtained included

trigger time, events, event number. During each test, cuttings were collected which were used to characterize drilling performance.

4.3.1 Review of Drilling Conditions

Drill-off tests were conducted on the medium strength concrete with rated rotary speed of 300 rpm. Fig. 8 shows the penetration time and depth when the applied WOB is 220.20 Kg. By converting axial vibration magnitude from time domain to frequency domain, the dominant frequency was found to be 4.5 Hz.

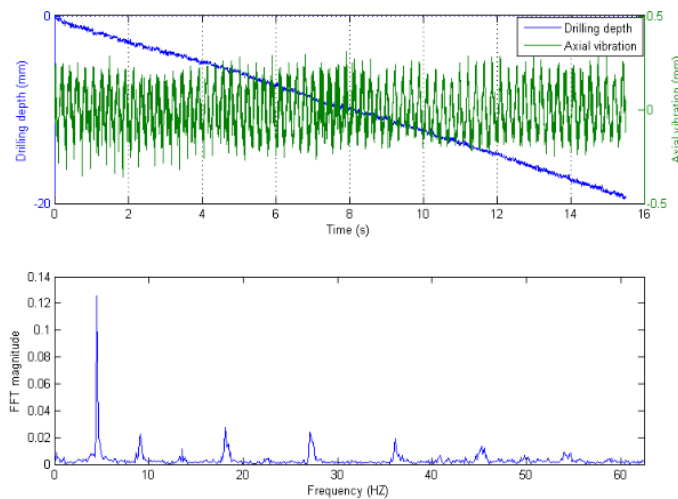


Figure 8 Rigid drilling when WOB = 220.20 Kg. PDC bit penetrates around 20 mm on medium strength concrete (upper left) and axial vibration magnitude varies with time (upper right). Vibration is converted from time domain to frequency domain (Lower).

4.3.2 Rock Penetration Characterization

Under laboratory conditions, applied WOB on drill bit varied from 220.20 to 515.65 Kg and corresponding ROPs were obtained (Figure 9). From this figure 9, ROP increases with increasing WOB for each setting. For the high WOB situation, the penetration rate with the strong compliance setting was the highest while the penetration rate under rigid setting was the lowest.

The intersection of the curves for rigid and medium compliance settings indicates that there is little difference in penetration rate under low WOB situations.

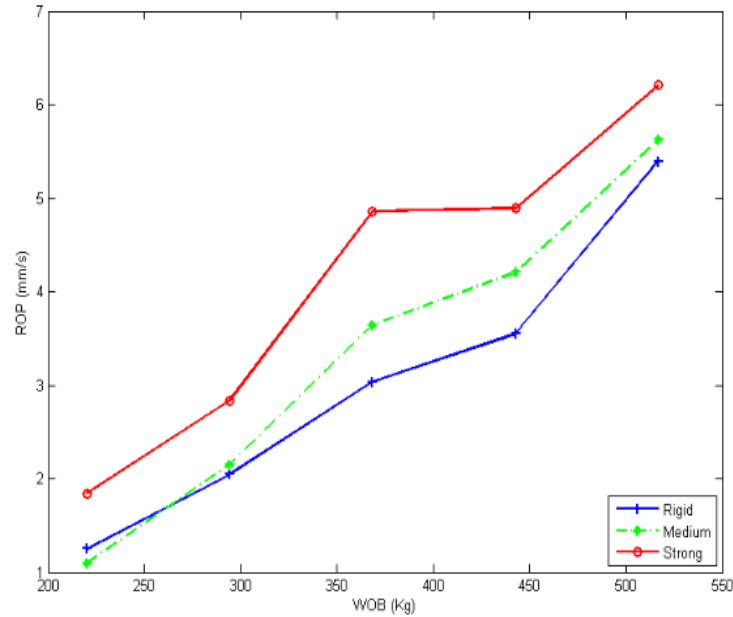


Figure 9 Laboratory rate of penetration (ROP) versus WOB under three different compliance settings.

To eliminate the effect of rotary speed on penetration rate, both rate of penetration and rotary speed were normalized to 300 rpm. Normalized ROP was obtained from the actual ROP multiplied by the ratio of the rated rotary speed over the actual one. The normalized rotary speed was the ratio of the actual rotary speed over the rated one. Normalized results are shown in Figure10. The rotary speed decreases with increased WOB and corresponding drag force on PDC bit cutter increases. The normalized ROP is higher than actual ROP for all WOB situations due to the slight decrease of rotary speed from the rated one.

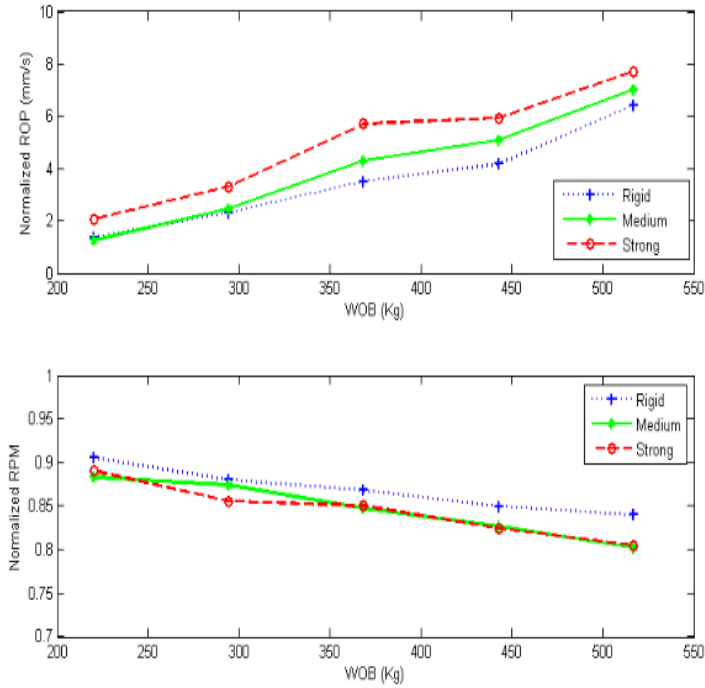


Figure 10 ROP is normalized to 300 RPM situation for eliminating the effect of different rotary speed (upper) and actual rotary speed normalized to 300 RPM (lower).

4.3.3 Cutting Analysis Results

Particle-size distribution charts are obtained for three different drilling settings in Fig. 11 in ranges from 10 micron to 2 millimeters. The vertical axis stands for the cumulative percentage that cuttings are less than indicated size. For any indicated sieve size, the lower the cumulative percentage, the higher percentage of cuttings is left in sieves. For any cumulative percentage, the higher of the size indicates bigger cuttings are obtained.

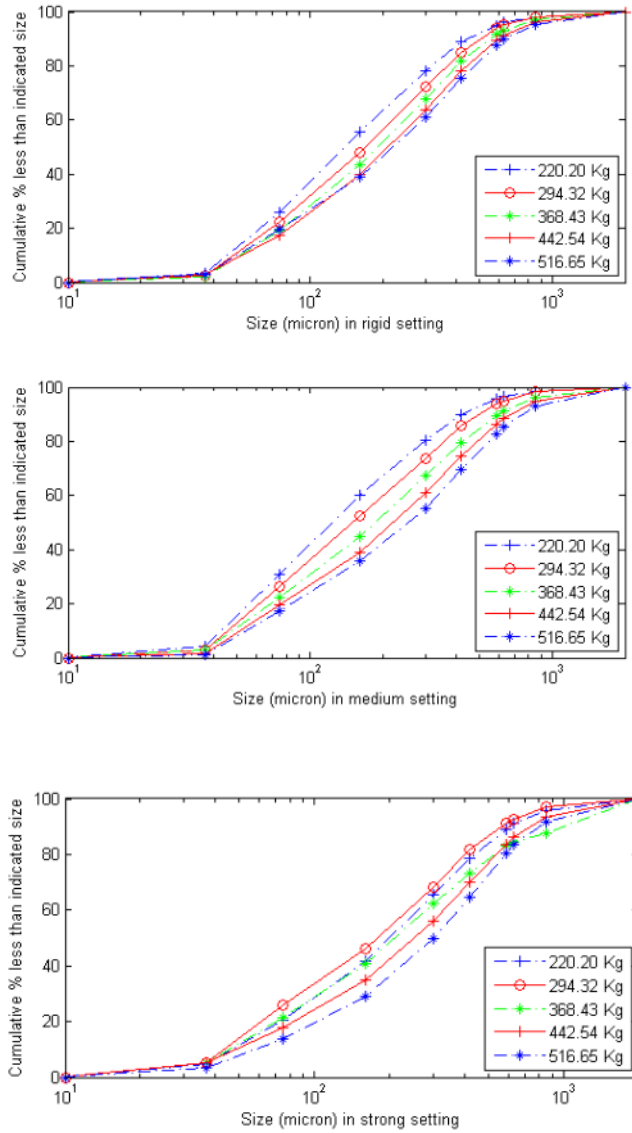
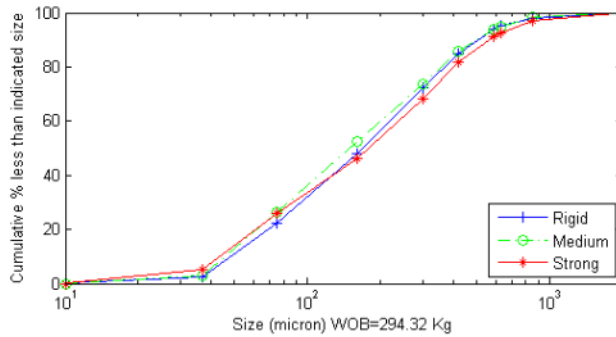
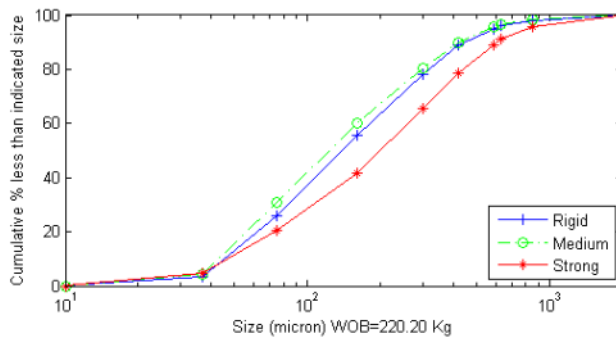


Figure 11 Particle-size distribution from drilling with rigid compliance (upper), medium compliance (middle) and strong compliance setting (lower)

From Figure 11, cuttings size is generally bigger with increasing of WOB for all rigid, medium and strong compliance settings. There is exemption on drilling with strong compliance setting. Cutting size with WOB of 220.20 Kg is bigger than that with WOB of 294.32 Kg. The general trend indicates that higher WOB tends to generate bigger cutting size.

Cutting size is also investigated for three compliance settings under the same WOB in Figure 12. In these figures, cutting size distribution is investigated for all five applied WOBs. For lower WOB situations such as 220.20 Kg and 294.32 Kg, strong compliance setting tends to generate bigger cuttings while rigid compliance setting generates bigger cutting than medium compliance. For larger WOB situations, stronger compliance settings tend to generate bigger cuttings.



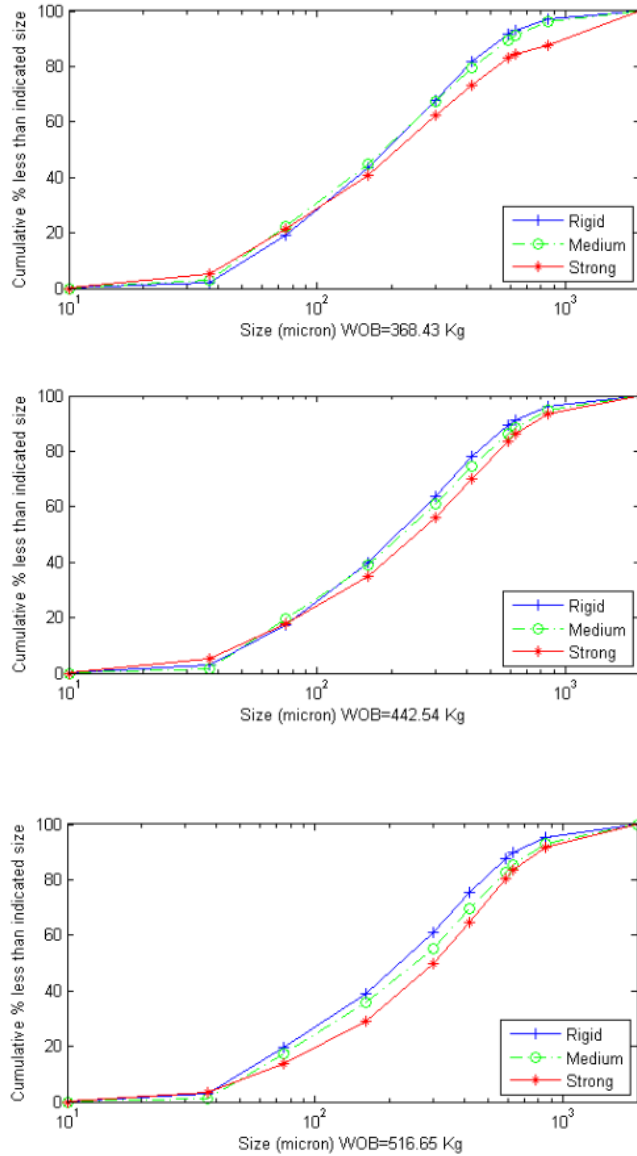


Figure 12 Particle-size distributions from different WOB

The reason for the dependence of the cutting size distribution on compliance setting changing with different WOBs is explained. The compliance system gives different responses to different axial force, i.e. WOB. The compliance system absorbs and converts the bit motion into axial displacement with little effectiveness at low WOB. And it works with higher effectiveness at higher WOB. An obvious role of different compliance on cutting size distribution was observed when WOB is above 294.32 Kg.

Cutting size was analyzed with a microscope at 16 X magnification. Some of the magnified cuttings were identified in Fig. 13. Cutting particles are comprised of aggregates such as siliceous siltstone and volcanic rocks, and concrete clump containing smaller aggregates. From these figures, particles sharpness decreases from large size to smaller cutting size. This indicates that bigger cuttings are re-grinded when bottom hole cleaning is not perfect.

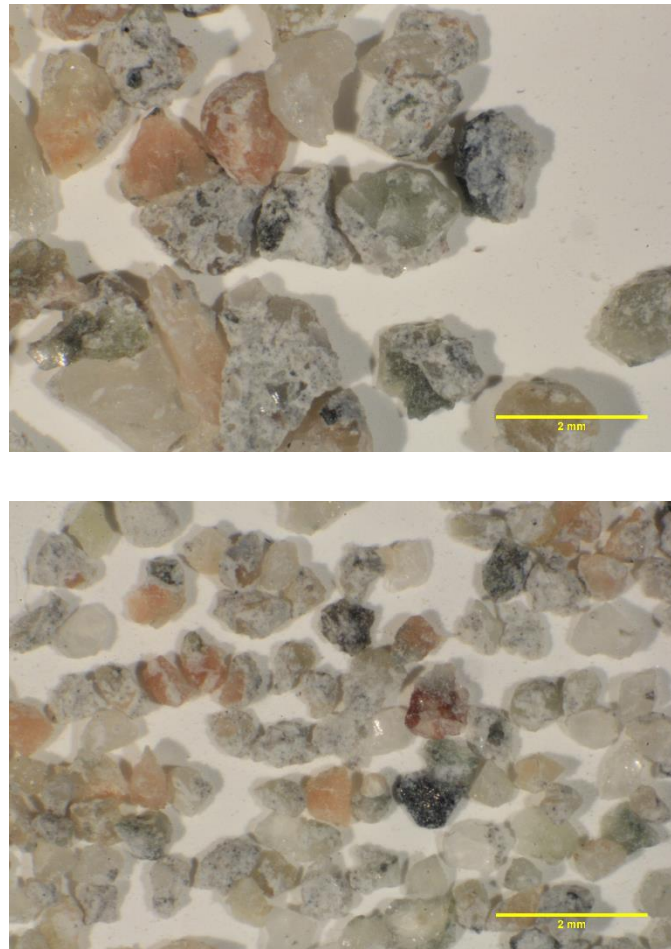


Figure 13 Particles obtained from drilling when WOB=516.65 Kg at strong compliance setting, whose size ranges from 850 to 2000 micron (upper) and from 420 to 590 micron (lower).

4.3.4 Acoustic Emission Results

Acoustic emission events were recorded during each run of drill-off test. A typical signal and its spectrogram analysis are displayed in Figure 14. The waveform shows transient

fluctuations of emissions power with respect to a background level. Each waveform lasts 1.6384 millisecond and comprises of 16384 points. The spectral content of the transient signals ranges from 50 to 300 kilo Hertz. Considering the drilling process, acoustic emission signal is comprised of rock cracking, system noise, drill rig vibration, etc. The cracking signal will not be solely extracted from the continuous waveform in this paper.

The acoustic emission event rate is calculated based on cumulative number of triggered events during a typical time window within each run of drill-off test. Also, the corresponding event energy is integrated from the event waveform on the time domain [29]. Then, the average event energy is obtained from this drilling window. Both event rate and average energy for the trigger channel are shown in Figure 14.

The average event energy increases with increase of WOB for all three compliance settings, and event rate slightly increases. Under the same WOB, the average event energy of rigid compliance setting is the largest and smallest magnitude of event energy is emitted from strong compliance drilling. The reason is that higher rate of events are generated in strong compliance settings than that in rigid setting.

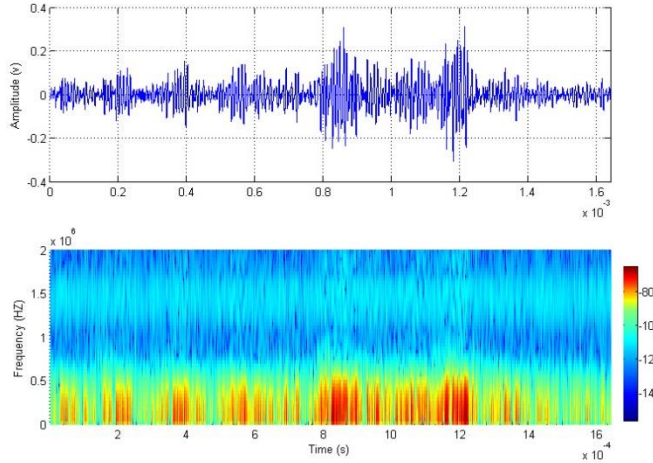


Figure 14 Single acoustic emission from rigid drilling when WOB= 202.20 Kg (upper) and spectrogram (lower).

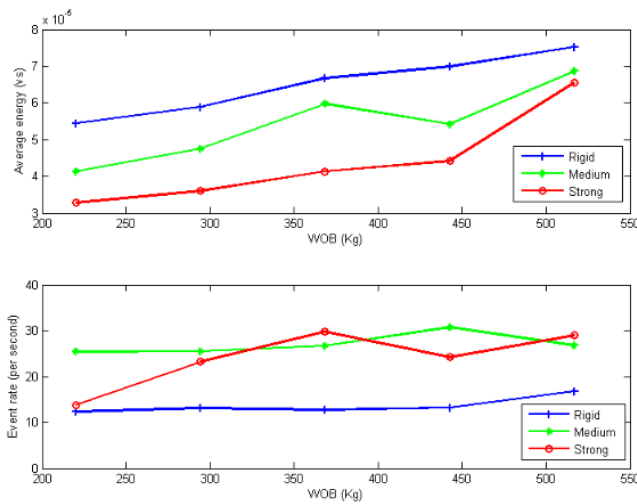


Figure 15 Average event energy (upper) and event rate (number of triggered events per second, lower) from the trigger channel.

4.3.5 Acoustic Emission and ROP

Some conclusions can be obtained by comparing the event rate and average event energy in Figure 16. With increasing ROP, the average event energy increases for all the three different complicate setting. This correlates with the previous cutting size distribution results. Bigger size

of cutting is generated with increase of ROP. In this way, higher average event energy correlates with bigger size of cutting, or in other words, larger crack surfaces during the drilling process.

Under the same ROP, the highest average event energy occurs in the rigid complicate setting while the lowest average event energy occurs at the strong complicate setting. The higher average event energy mainly originates from a lower event rate generated with less compliant setting as shown in Figure16.

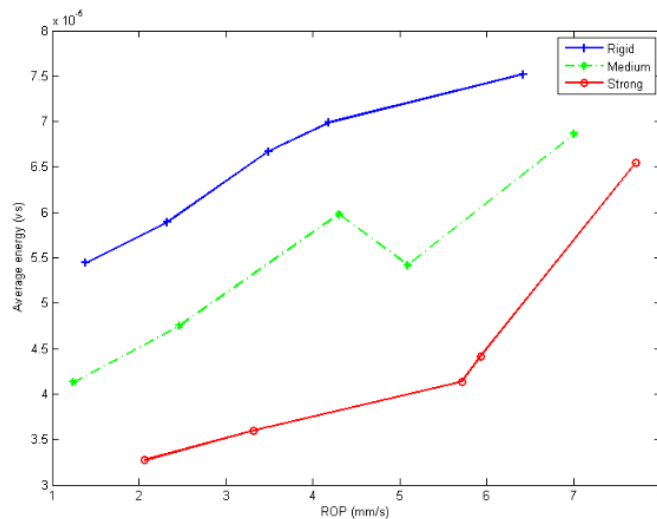


Figure 16 Average event energy versus ROP under three different complicate settings.

4.4 Discussion and Conclusions

Rate of penetration increases with increase of applied WOB. A stronger compliance setting helps to improve drilling performance compared to rigid drilling setting.

Cutting size distribution correlates with improved rate of penetration. The higher the WOB, the cutting size is bigger. Also, a stronger compliance setting drilling increases ROP by increasing cutting size for each size range.

Higher average event energy correlates with higher ROP with increase of WOB, which corresponds to bigger cutting size and higher event rate.

Under the same WOB condition, average event energy is reversely correlated to compliance setting. Stronger compliance tends to generate lower average event energy due to higher event rate.

Chapter 5 DEM Simulation of Enhancing Drilling Penetration Using Vibration and Experimental Validation

This chapter is the paper “DEM Simulation of Enhancing Drilling Penetration Using Vibration and Experimental Validation” authored by Jinghan Zhong, Stephen Butt and Jianming Yang, and was published in the Proceedings of the 2016 summer simulation multi-conference, Montreal, Quebec, Canada. The MEng candidate was involved with the planning and execution of the drilling experiments, the experimental data analysis, and the writing of the paper.

Abstract

This paper details a study of Discrete Element Method (DEM) simulation of drilling penetration and is part of a broader investigation of the influence of bit vibration and rock-cutter compliance on enhancing drilling performance. It has been shown from laboratory experiments and field drilling trials that axial bit vibration (induced by modulated bit-rock compliance) can play a positive role in improving drilling rate of penetration (ROP), and the Drilling Technology Laboratory (DTL) at Memorial University of Newfoundland has incorporated this into passive Vibration Assisted Rotational Drilling (pVARD) technology and drilling tools. This paper focuses on DEM simulation of polycrystalline diamond compact (PDC) bit penetration and experimental validation of drilling with and without the pVARD technology, all other factors

being equal, as a means of both evaluating the pVARD technology and understanding the basis of enhancing drilling performance. Simulated axial vibration properties such as amplitude and frequency were adjusted with different settings of spring compliance and dampening layers, simulating the physical configuration of the pVARD tool used for laboratory experiments. Mechanic Specific Energy (MSE), Material Removal Rate (MRR) and Depth of Cut (DOC) are calculated to evaluate drilling performance and efficiency, and are used to compare the pVARD and non pVARD drilling results. In general, the DEM simulations agree with the experimental drilling results, and both indicate improved drilling performance using the pVARD technology.

5.1 Introduction

Drilling quickly to hydrocarbon formations is one of the major targets in the oil and gas drilling industry. Vibration drilling has been proven to be able to dramatically increase the rate of penetration (ROP) both in the laboratory and field conditions [38]. Researchers in Drilling Technology Laboratory at Memorial University have been working on new vibration drilling tools that effectively improve drilling performance based on physical and numerical simulation [40, 12]. Active vibration has been generated using a hydro pulse vibration tool that was driven by high pressure fluid [41]. A new vibration tool was designed and tested in drill-off tests with passively generated vibration during drilling [37]. In this paper, the Discrete Element Method (DEM) numerical simulation of the bit-rock interaction was used to evaluate the drilling performance of this tool.

Drilling performance is evaluated by parameters such as rate of penetration (ROP) and mechanical specific energy (MSE) [41] and material removal rate (MRR) [42]. Within a PFC2D (Particle Flow Code in 2Dimensions) model, drilling performance is characterized by MSE,

depth of cut (DOC) and MRR [39, 40]. Material removal rate is proportional to drilling rate of penetration, while mechanical specific energy is a measure of energy consumed per unit volume drilled, and, in general, increased removal rate and/or lower mechanical specific energy are an indication of improved drilling performance.

In short, many drilling tests were finished, not only in the Advanced Technology Laboratory (ATL) in which load on cutters can be increased. Laboratory experiments were conducted with various loads, with the same cutting area, cutting speed, back dip angle of PDC cutter and same rock properties. The experimental results were analyzed with multiple nonlinear regression technique and a new cutter and rock interaction model was proposed. The results show that the force on the cutter (half of the WOB) and passive vibration are the principal factors influencing the cutting efficiency, rate of penetration and drilling performance. Interaction model of PDC cutter and rock are set up by DEM model, combining with the PFC model and bit rock interaction model from previous research. Also, a new model which adds spring stiffness and damping coefficient and could completely simulate the new passive vibration tool was set up.



Figure 17. Laboratory drilling system [39].

5.2 Laboratory Drill-Off Tests

5.2.1 Drilling Tests

Laboratory drilling was done using the instrumented drilling system shown in Figure 17. In the experiments, a 2 cutter 35 mm diameter polycrystalline diamond compact (PDC) drill bit was used to drill fine-grained concrete samples with properties similar to low permeability sedimentary rock. All drilling was done using the same near-atmospheric bottom-hole pressure,

drilling fluid flow rate, and corresponding bit hydraulics. Rock parameters in the DEM simulation were similar to the parameters in the lab tests [43].

Compliance was present in the pVARD tool, which was assembled above the drill string. The bit vibration was monitored using a laser sensor, drilling depth was monitored using a linear variable differential transformer (LVDT), and weight on bit was monitored using a load cell. All the parameters were recorded automatically during the drilling process using an electronic data acquisition system.

Two groups of drill-off tests were conducted: rigid (non pVARD) and compliance (pVARD) drilling. Fine grained concrete cylinders were used for drilling specimens, 8 inch in height and 4 inch in outer diameter, with unconfined compression strength of 46 MPa. Tap water was used to clean the bottom-hole cuttings at atmospheric pressure.

As mentioned in the previous chapter, the lab scale bit is two cutters bit. Inputs that were varied include weight on bit (WOB) and compliance, which control the spring stiffness and damping coefficient. Drilling performance was evaluated through rate of penetration (ROP), mechanical specific energy (MSE), material removal rate (MRR) and depth of cut (DOC). [44].

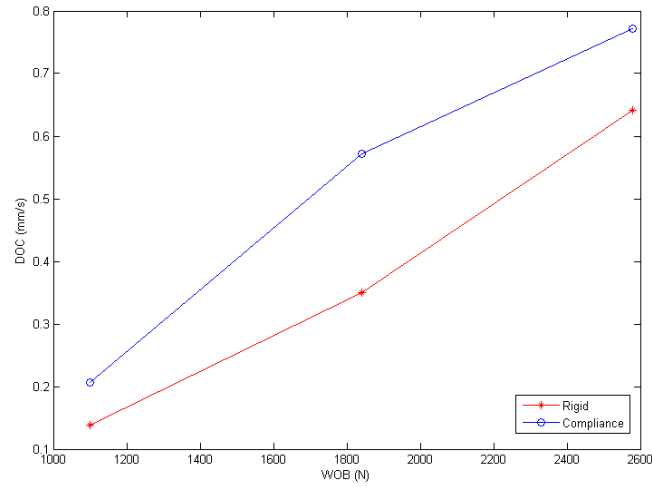


Figure 18 Single cutter DOC versus WOB for two drilling settings.

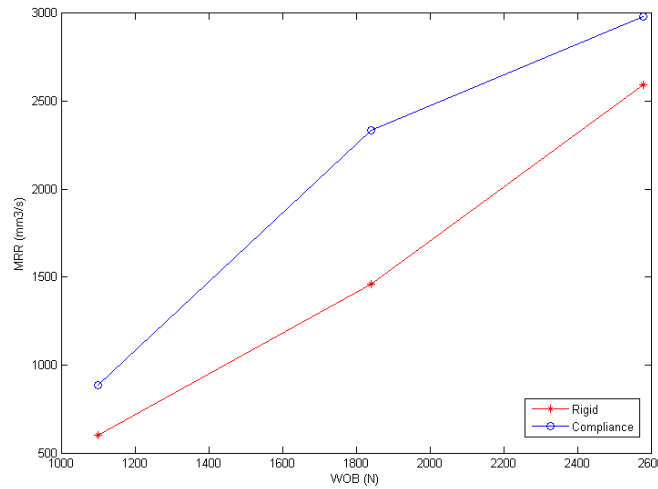


Figure 19 MRR versus WOB for two drilling settings.

The third indicator is MSE, which is empirically obtained [38] using

$$MSE = \frac{WOB}{A_B} + \frac{120\pi \times N \times T}{A_B \times ROP} \quad (5.1)$$

$$T = \mu \frac{D_B \times WOB}{36} \quad (5.2)$$

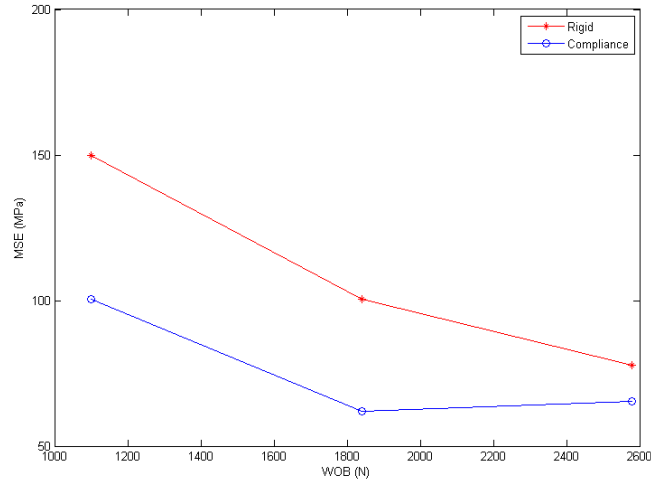


Figure 20 MSE versus WOB for two drilling settings.

5.3 Numerical Simulation

A numerical model was constructed to simulate the cutting process using Particle Flow Code (PFC2D). In this model, the material is represented by a flat-joint model that more precisely represents the drilled material for small scale fracturing processes [45].

5.3.1 Material Calibration

The PFC2D material is modeled as a series of small balls with a specified size distribution and contact strength and stiffness. Material calibration is conducted using a built-in library function which adjusts ball scale material properties to achieve macroscale properties such as tensile strength (σ), unconfined compressive strength (UCS), and confined compressive strength (CCS) (Figure 21). First, in the UCS test, Young's modulus, Poisson's ratio and bond tensile strength are adjusted in order. Second, bond tensile strength is adjusted to make bond cohesion match the parameters above in the UCS test. Last, increase bond friction angle to fit with CCS or Mohr's friction angle.

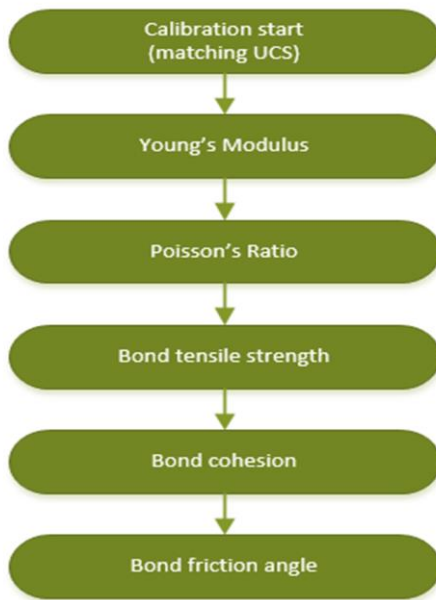


Figure 21 Calibration process of PFC2D model.

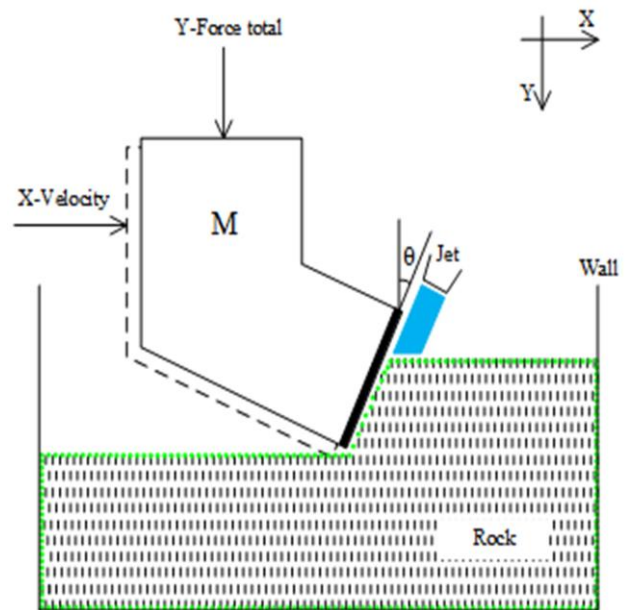


Figure 22 Illustration of PDC bit cutting process.

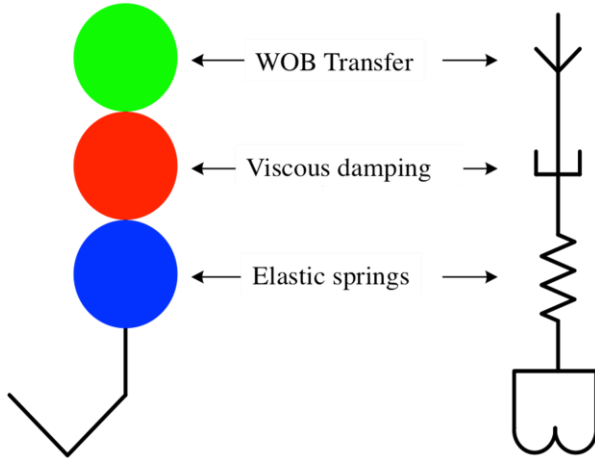


Figure 23 PVAR tool illustration and simplification.

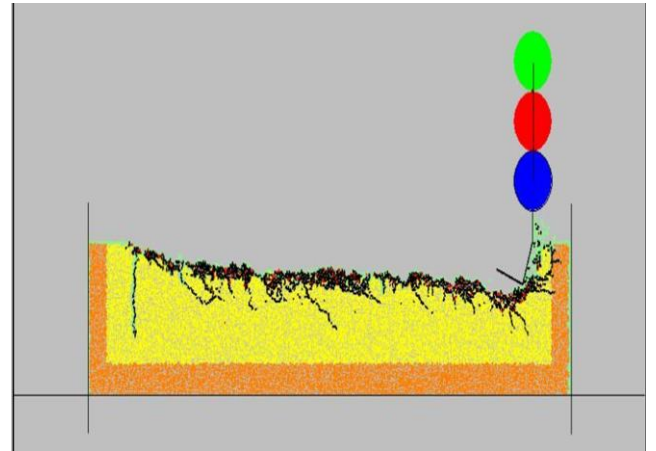


Figure 24 Single cutter cutting process.

5.3.2 Model Construction

The single cutter PFC2D models were based on the single cutter drilling scenario described in chapter 4. The PDC cutter back rake angle θ was 20° [46]. The p-VARD vibration tool is divided into three sections (From the top to the bottom): WOB transfer (top), dampening tool (middle) and spring tool (bottom), shown conceptually in Figure 23. For DEM simulation, the tool is simplified into static WOB, damping, and elastic compliance sections. Figure 23 shows a representative simulation of a single cutter penetrating the model material.

This modeling used the forces equation:

$$Mq''(t) + Cq'(t) + Kq(t) = F_0 \quad (5.3)$$

Where M , C and K are the system's global mass, damping and stiffness matrices, respectively, and α and β are constants defined by critical damping of the chosen virtual material.

$$C = \alpha M + \beta K \quad (5.4)$$

Since cutter horizontal speed is constant, only the Y position force is computed using

$$F_y = Mg + K_y y(t) + C_y \dot{y} \quad (5.5)$$

And, the value of C_y and K_y , which stand for damping coefficient and spring stiffness respectively, come from lab test on the rubbers and springs in the tool. After calibration, $C_y=2 \times 10^3 \text{ N.s/m}$, $K_y=2 \times 10^6 \text{ N/m}$ are used.

In Figure 24, the three colored balls stand for three different sections of the pVARD tool. The first section is WOB from the drill string weight and applied weight from a suspended mass. The second ball represents the dampening tool which is the significant part in the whole P-VARD tool. In the simulation, one of the control conditions, the dampening stiffness changes from $2.0 \times 10^3 \text{ Ns/m}$, as with our lab data, to $2.0 \times 10^{20} \text{ Ns/m}$ similar to a steel plate. In addition, the lowest portion of the tool before cutters is a vibration tool that consists of elastic springs that transfer the axial force while allowing axial vibration to occur. The single cutter cutting trace is demonstrated in Figure 25.

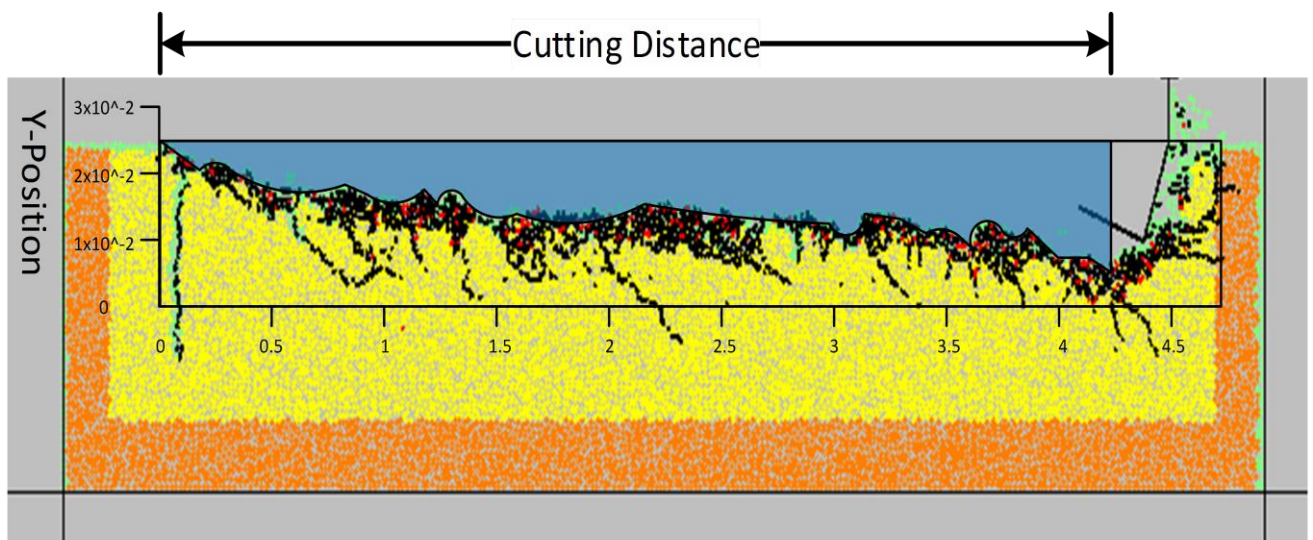


Figure 25 Illustration of cutting area to measure the DOC and MRR.

5.3.3 Simulation Results

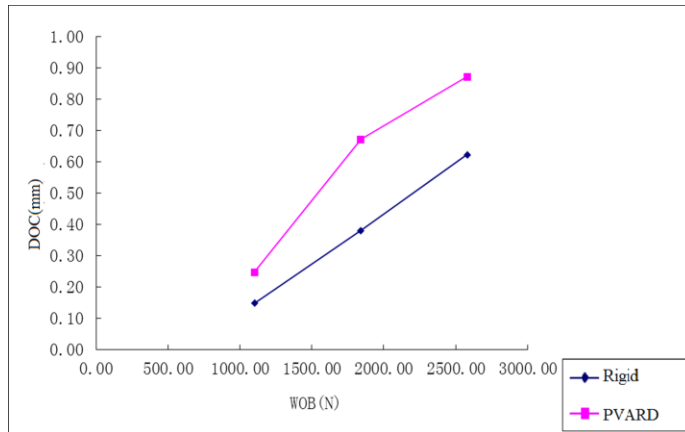


Figure 26 DOC versus WOB (simulation).

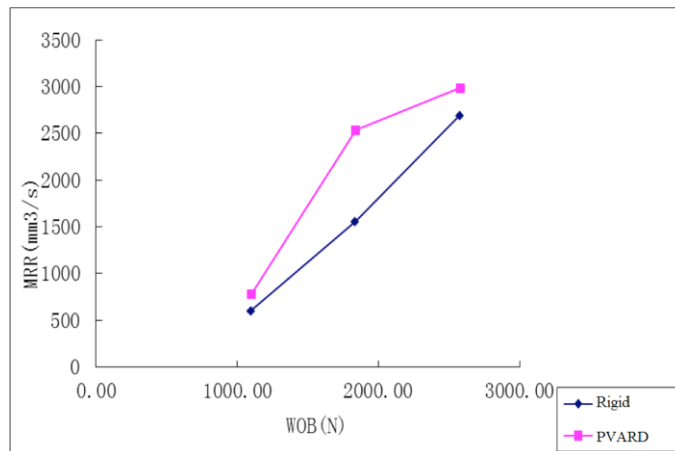


Figure 27 MRR versus WOB (simulation).

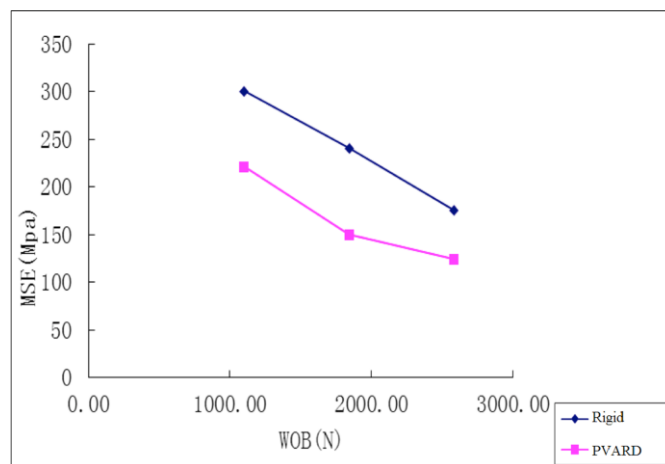


Figure 28 MSE versus WOB (simulation).

To evaluate the cutting performance in the simulation results, the parameters compared to the experimental results are the depth of cut, material removal rate and mechanical specific energy. The depth of cut is directly obtained from the cutter's deepest Y-position during this X distance plot as in Fig. 25. To measure the material removal rate, the blue shadow area is the removed material volume. This area is integrated from the cutter Y-position versus X-position plot. The removal rate is calculated from the following formula.

$$MRR = \frac{\text{Removed Volume}}{\text{Cutting Time}} \quad (5.6)$$

Where Removed Volume is the removed volume of the cutter in the simulation, and Cutting Time (CT) is the single cutter cutting time in the simulation. MSE was calculated from the following formula [41].

$$MSE = \frac{\text{Work Done in Cutting Action}}{\text{Volume of Rock Cut}} = \frac{\int(\text{Force})dx}{\text{Volume of Cut}} = \frac{\sum_{t_1}^{t_2} F_x \cdot \Delta X}{Z \cdot \sum_{t_1}^{t_2} Y \cdot \Delta X} \quad (5.7)$$

The simulation results are shown in Figs. 26 to 28 for depth of cut, material removal rate and mechanical specific energy. In all instances, the drilling performance for pVARD drilling is better than the corresponding results for the rigid drilling. As well, the results approximate the laboratory drilling results given in Fig18 to Fig20. To validating the DEM models for simulating the penetration process and the pVARD tool actions. The simulation results are agreed with all experiment data, except the Y-axis values of MSE. This is because hydraulic factors, which represents as the flow rate in experiment, could not be taken into consideration in the simulation. Hence, the MSE value of simulation in Fig. 28 is a little higher than experiment result in Fig. 20. It is because the real lab test has double cutter drilling bit, while the DEM simulation only has single cutter drilling performance. Although these two cutters are in the same bit, this difference does not influence the depth of cut and the removal rate. There are other reasons, like the

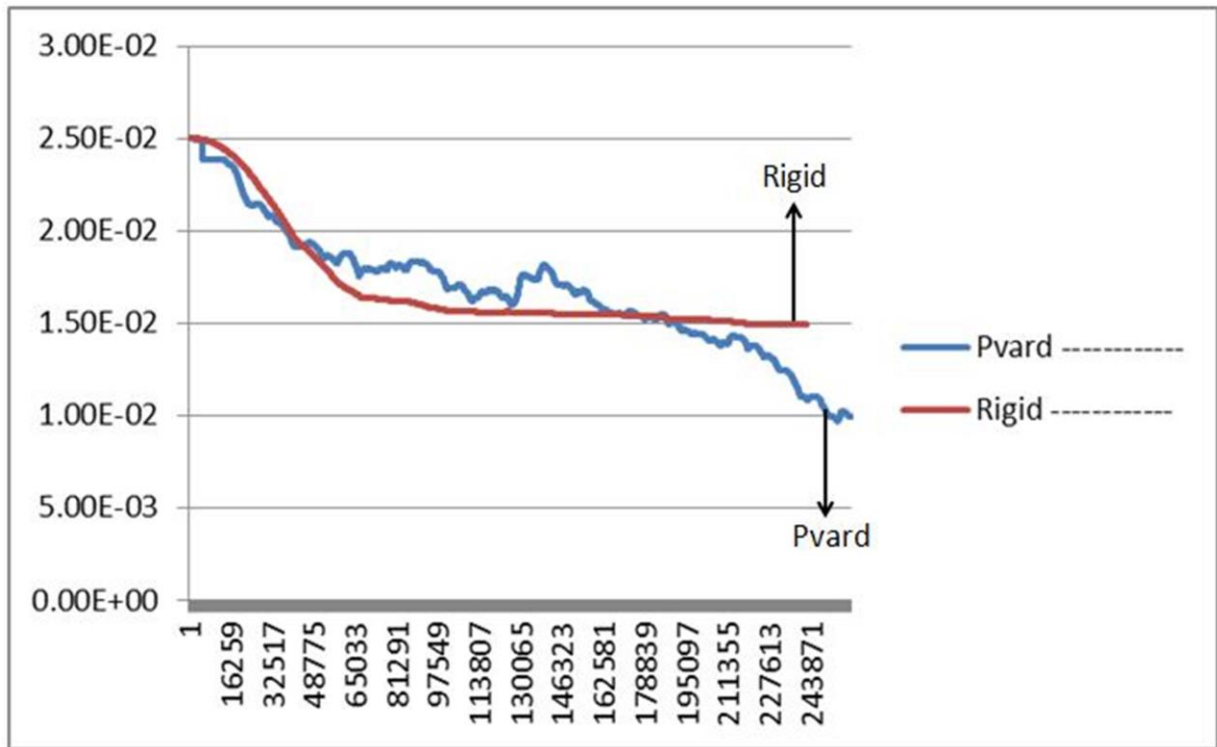


Figure 29 Y-position (mm) vs time (10-1sec) for rigid and pVARD, two simulations at WOB of hydraulic factors or bottom hole pressure, could cause result in this energy consumption difference, which is reflected in MSE. However, they are all within reasonable range and have same trend, it is obvious that rigid drilling requires more energy than drilling with pVARD tool.

Further evaluation of the simulation results provides insight into the actions of the axial compliance and dampening functions of the pVARD tool. Fig. 29 plots the Y-position of the cutter for the drilling simulations at WOB of 2500 N for both rigid and pVARD drilling. From these data, it is evident that the pVARD drilling penetrated deeper into for the same lateral traverse distance (since the rate of X-position increase is constant). This accounts for the higher depth of cut and material removal rate for the pVARD simulations, and since all other drilling parameters were the same, the corresponding lower mechanical specific energy. As well, the y-position for the pVARD has many more small vertical oscillations than the rigid drilling, indicating the actions of the pVARD tool elements to generate bit vibrations.

5.4 Conclusions

In this part of research, the DEM simulations were used to model the drilling performance of rigid and pVARD drilling and compared with corresponding laboratory drilling results with comparable parameters. Overall, the DEM simulations agree with the experimental results in the lab, and both indicate that the pVARD drilling had improved drilling performance compared to non pVARD drilling, all others drilling parameters being the same. Further DEM analysis confirmed that the configuration of the pVARD tool acted to induce small amplitude vibrations at the bit-rock interface.

Chapter 6 Characterization of the Dynamic Compliance for the Passive Vibration Assisted Rotation Drilling (pVARD) Tool

This chapter is the paper authored by Jinghan Zhong, Stephen Butt, and Jianming Yang .It has been prepared for submission to a journal. The MEng candidate was involved with the planning and execution of the drilling experiments, the experimental data analysis, and the writing of the paper.

Abstract: A series of drilling experiments were carried out by the DTL (Drilling Technology Laboratory) using a new experimental equipment, which was named passive Vibration Assisted Rotation Drilling (pVARD) tool. To understand how the specific springs and the rubbers work in the new drilling tool and how they help to improve the rate of penetration in drilling by applying the passive vibration to the bit and drill pipe, the author based on the previous vibration tool testing of the rubber and spring to invent a new testing method. Due to several vibration analyses of the passive vibration assisted rotation drilling, and in order to set up the future Discrete Element Method (DEM) modeling with analytical validation, we should know the accurate numerical value of the damping coefficient and the spring stiffness of the drill string of the new tool. Experiments were conducted in the mechanical laboratory, which has been designed to test the PVAR tool inside frequency-dependent spring stiffness and damping parameters of the specific springs and the rubbers. A hydraulic actuator was set up to apply different frequencies and amplitudes by the isolator. The bottom part of the isolator is a steel

plate, which could hold the rubber or springs to fluctuate on the vertical direction; the top part of the isolator is fixed on the actuator frame. Both sides of this hydraulic actuator have sensors to record the force and displacement changes, so it can translate the frequencies from 4.5 to 19 HZ and amplitude range from 0.5mm to 2mm, which match the real pVARD tool field work condition. The slope of the test graph (force vs displacement) is calculated to obtain the spring stiffness. Then, the spring component force is eliminated from the total force, and only the damping force part is left. There are two methods to compute the damping coefficients, one is to use the slope of the force-velocity curves same as the method of spring stiffness, and another is directly using the damping part equation to divide the velocities from the based dynamic total force equation to calculate the damping coefficient. The spring stiffness was proved by the static state deflection tests and the two methods calculations of damping coefficient are in agreement with each other. The empirical formula was developed to estimate this new drilling tool damping and spring parameters under different amplitudes and frequencies. The damping and spring parameters are used in the DEM simulation of the pVARD tool and show an ideal increase of the ROP, which agree with the real field trail testing.

6.1 Introduction

To increase the drilling efficiency and the rate of penetration (ROP), a new Passive Vibration Rotation Drilling (P-VARD) tool was developed by the advanced Drilling Technology Laboratory. The field application shows that this technology can solve the contradiction and conflicts among rate of penetration (ROP), weight of bit (WOB) and bottom hole pressure (BHP) under normal drilling conditions and the drilling efficiency can be increased dramatically. So, how to calculate damping coefficient and spring stiffness of the new tool is becoming a crucial problem to the research on the evaluation of the new tool's drilling efficiency and these two

significant parameters need to be inputted into the later DEM single cutter pVARD tool simulation.

Due to the importance of the mechanical vibration in the drilling tool, several studies have been done to understand the passive vibration of the drillstring. In the past couple of years, there are several relevant literatures that were published on spring and damping coefficient testing or vibration tool designed, but seldom to be taking into consideration and used in drilling and oil exploration.

The following section describes how this experiment is set up and what kind of specific damping rubbers and springs were used in this tool. Section 3 presents how to calculate the springs and damping coefficient. Based on the force and displacement data, section 4 provides the experiment result, such as the tests matrix, a typical example of how to calculate the damping and spring using the method and formula in section 3, and presents a new equation model of specific spring stiffness and damping coefficient under the different frequencies and amplitudes. Section 5 gives a brief description of the DEM model of the pVARD tool which uses the specific spring stiffness and damping coefficient which was test in this experiment and shows sample results. The Y position forces that are transmitted to the rock and to the frame are plotted under real field trail frequency response functions. Conclusions and future work are given in Section 6.

6.1.1 Experiment Setup and Materials of Equipment

A hydraulic actuator was set up to test the specific rubbers and springs, which were used in the new drilling tool (Fig30). The vibratory force was acted on the rubbers or springs at the frequencies ranging from 4.5 to 19 HZ, which is close to the real field work drilling frequencies and the amplitudes are set from 0.5mm to 2mm depending on the different length of the rubber

rings or spring rings. The frequencies and amplitudes were all inputted in the computer software, which is called LabView and it also could record the force and displacement. (Both the frequencies and amplitudes are set in the computer software). (Fig31).



Figure 30 Testing equipment set up with two parts of isolator and load is control by a hydraulic actuator

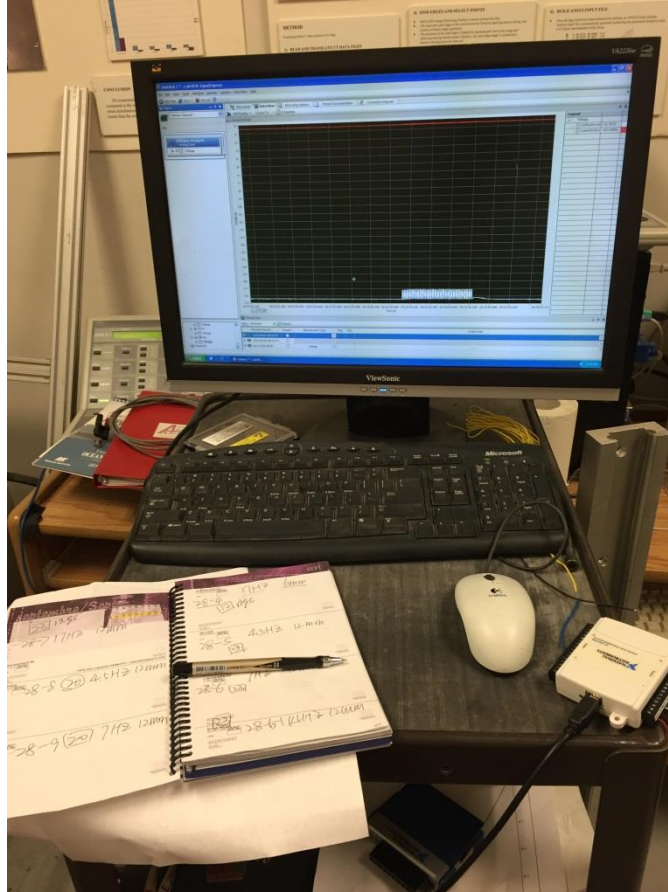


Figure 31 Recording computer and input/output national instruments analog (NI USB-6009)

In this experiment, Buna-N (Nitrile) rubber was used as the damping material, known as: acrylonitrile butadiene rubber as well. The general purpose of this molded o-ring material is because it has relative economical, excellent mechanical properties and basic resistance to many common lubricants. Specific physical and chemical resistances vary by compound formulation. It is also resistant to compression set and tear/abrasion. In summary, Buna-N rubber has many compound variations designed and strengths to meet specific applications. In the real field pVARD tool, 24 rings of Buna-N 40A rubber were used inside the tool and each is about 13.5mm thickness. In addition, 30 rings of Belleville spring washers were stacked to form the spring assembly in the field trail real pVARD tool. In this case, the Belleville spring washers used high-

carbon steel Belleville dis springs. Its minimum Inter Diameter (ID) is 0.755", maximum Outer Diameter (OD) is 1.5", thickness is 0.045", height is 0.093". Since the springs add each other in parallel and take the lab safety into consideration, we only set up 1 to 6 spring rings (Fig.32) to test and the spring stiffness of 30 springs could be calculated by the mathematical method.



Figure 32 Rings of high-carbon steel Belleville dis springs are under tests

The following equation shows the energy loss per cycle in a damper in a harmonically forced system. In the classical mechanics [46,47], the system's relative force work is:

$$W_d = \oint F_d dx$$

Where F_d is the damping force. In viscous damping, $F_d = C\dot{x}$. Here we have the steady-state solution equation:

$$x = X \sin(\omega t - \phi)$$

So, after integration from left and right:

$$\dot{x} = \omega X \cos(\omega t - \phi)$$

Hence, we have

$$W_d = C\omega^2 X^2 \int_0^{\frac{2\pi}{\omega}} \cos^2(\omega t - \phi) dt = \pi C\omega X^2$$

At resonance frequency, the relationship between damper force, displacement and energy dissipated can be easily expressed as

$$W_d(\omega_n) = 2\zeta\pi K X^2$$

Where $\omega = \omega_n = \sqrt{\frac{K}{M}}$ and $C = 2\zeta\sqrt{KM}$. Recall the previous equation, we have

$$\dot{x} = \pm\omega X \sqrt{1 - \sin^2(\omega t - \phi)} = \pm\omega \sqrt{X^2 - x^2}$$

The damping force is

$$F_d = C\dot{x} = \pm C\omega \sqrt{X^2 - x^2}$$

Change both sides form, the equation becomes:

$$\left(\frac{F_d}{C\omega X}\right)^2 + \left(\frac{x}{X}\right)^2 = 1$$

And then,

$$C_{eq} = \frac{W_d}{\pi\omega X^2}$$

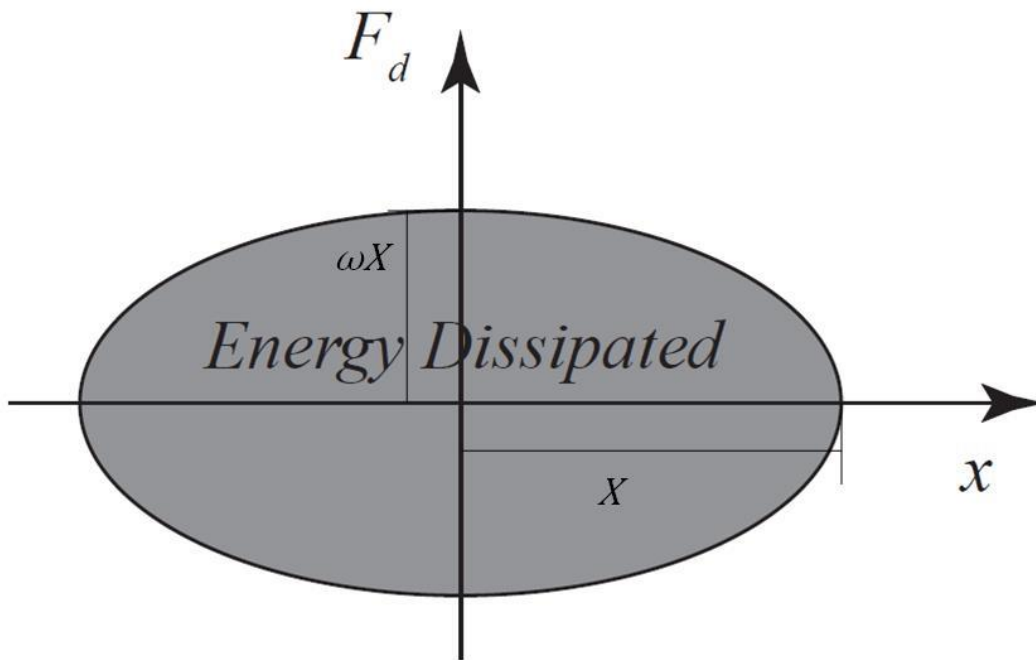


Figure 33 Work diagram: damping force VS displacement [47]

As is shown in Fig33 the work diagram are units are (N. m), and the denominator units are (m²/s), so the overall damping coefficient units are N.s/m.

Table6 and Table7 list all the experimental tests of the rubber O-rings and springs in the pVARD tool. The amplitudes and frequencies are selected according to previous DTL group's field trail tests. Meanwhile, the low amplitude below 0.5 has no obvious change on the actuator vibration. Also, high frequencies are out of the range, which is dependent on the value from

previous tests. Hence, it is not reasonable and high amplitudes are impossible in the lab test equipment (the rubber will fly off and the range is not reasonable).

Table 6 Tests matrix of the pVARD tool rubber's O-rings

| Rings of rubber | Frequency | Amplitude | The test result |
|------------------------|---------------------|-------------------|---|
| 1 | 4.5Hz,7Hz,17Hz,19Hz | 0.5,1mm,1.5mm | ideal |
| 2 | 4.5Hz,7Hz,17Hz,19Hz | 1mm,1.5mm,3mm | ideal |
| 3 | 4.5Hz,7Hz,17Hz,19Hz | 1.5mm,3mm,4mm,5mm | ideal |
| 6 | 4.5Hz,7Hz,17Hz,19Hz | 6mm | ideal |
| 12 | 4.5Hz,7Hz,17Hz,19Hz | 6mm | low frequency ideal(too high the rubbers fly) |
| 20 | 4.5Hz,7Hz,17Hz,19Hz | 6mm | low frequency ideal |
| 23 | 4.5Hz,7Hz,17Hz,19Hz | 6mm | low frequency ideal |

Table 7 Test matrix of the pVARD tool Springs

| Rings of springs | Frequency | Amplitude | The test result |
|-------------------------|---------------------|---------------------|---|
| 1 | 4.5Hz,7Hz,17Hz,19Hz | 0.5mm,1mm | ideal |
| 2 | 4.5Hz,7Hz,17Hz,19Hz | 0.5mm,1mm,1.5mm | ideal |
| 3 | 4.5Hz,7Hz,17Hz,19Hz | 0.5mm,1mm,1.5mm,2mm | ideal |
| 4 | 4.5Hz,7Hz,17Hz,19Hz | 0.5mm,1mm,1.5mm,2mm | ideal |
| 6 | 4.5Hz,7Hz,17Hz,19Hz | 0.5mm,1mm,1.5mm,2mm | Ideal for heavy load. If add more than these, it will too dangerous |

The data of displacement, force and velocity vs. time were subtracted by their mean values, followed by high-pass filtering. The effect of raw record data and filtering on sample is shown in Fig.34, with a vibration frequency of 19 Hz and displacement amplitude of 2 mm for each ring. The diagram of total force was generated according to these values. This generated diagram is

then used to estimate the spring stiffness. In order to find the damping coefficient, the stiffness component was subtracted from isolator force with the slope of the force-velocity curves and the area.

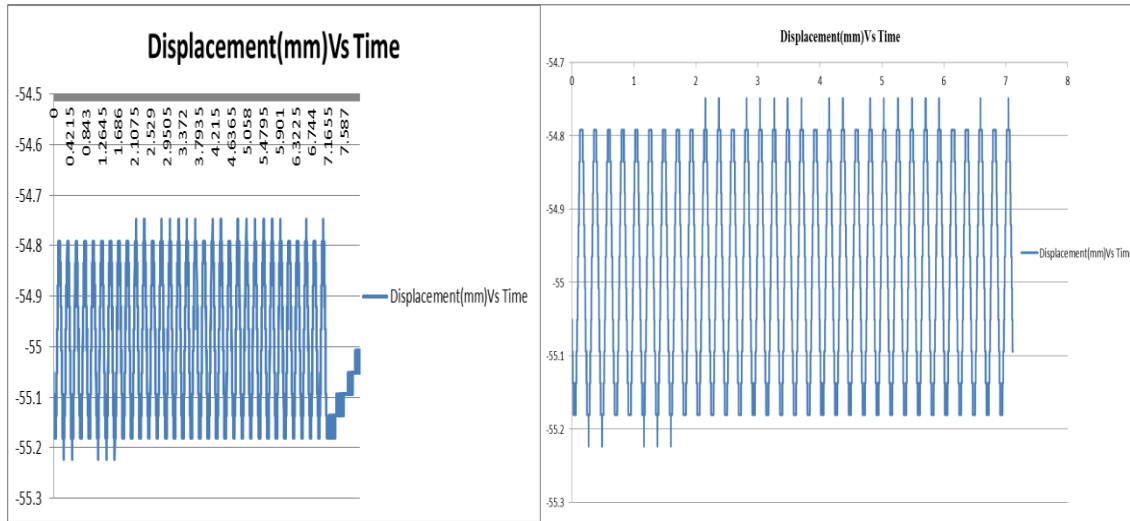


Figure 34 Effect of the raw record data (Left) and after filtering data (Right) on 15kN load, 2mm amplitude and 4.5Hz 6rings springs.

The process of the damping calibration is shown in Fig35 and Fig36. First, the spring constant is the slope of the curve, force versus displacement, in the Fig35. The slope K can be calibrated and the displacement is given, so the spring force can be obtained in this step. The second step is to find the area of the damper force. The damper force is the result of the total force minus the spring force. In addition, the Fig36 has revealed that the damper force versus the velocity where the slope of the curve defines the damping coefficient of this test.[47]

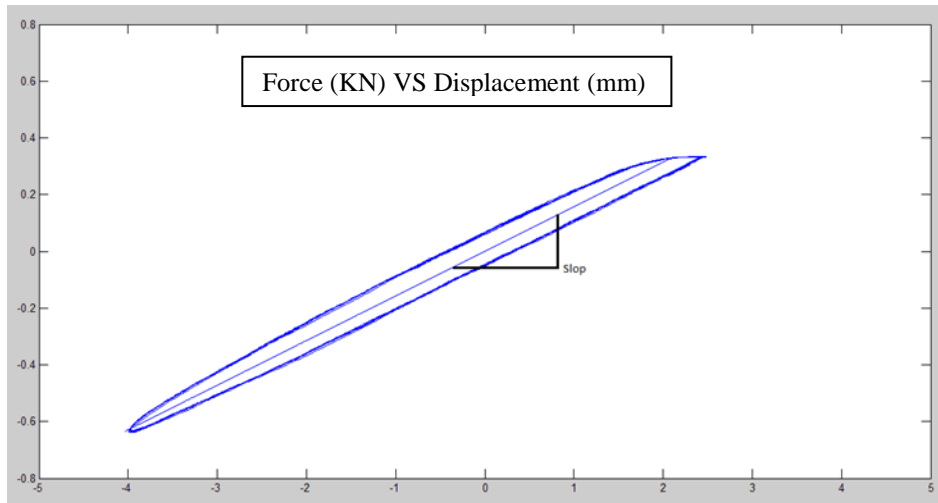


Figure 35 Springs constant, the slope of the dashed line

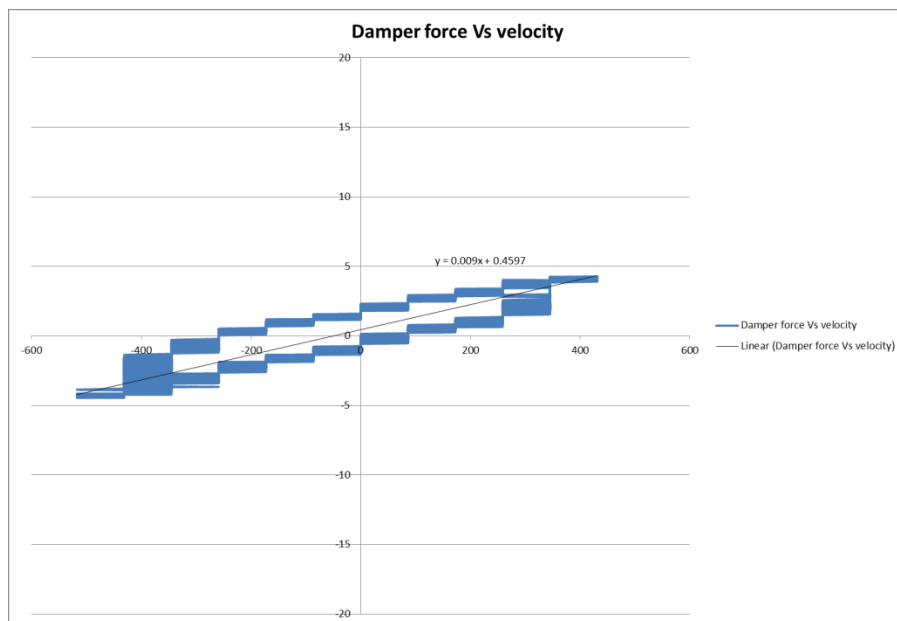


Figure 36 Damper force (KN) versus velocity (mm/s)

In summary, in the Fig36 we can see that, the slope of the damper force versus velocity can give the damping coefficient of the test material.

At each frequency and amplitude, the corresponding spring constant and damping coefficient can be found. To predict stiffness and damping, a response surface and regression model was then developed with the spring constant and damping coefficient. Fig.37 and Fig.38

show the response surface and the regression equations. The points in the figures are the values of spring constant and damping coefficient.

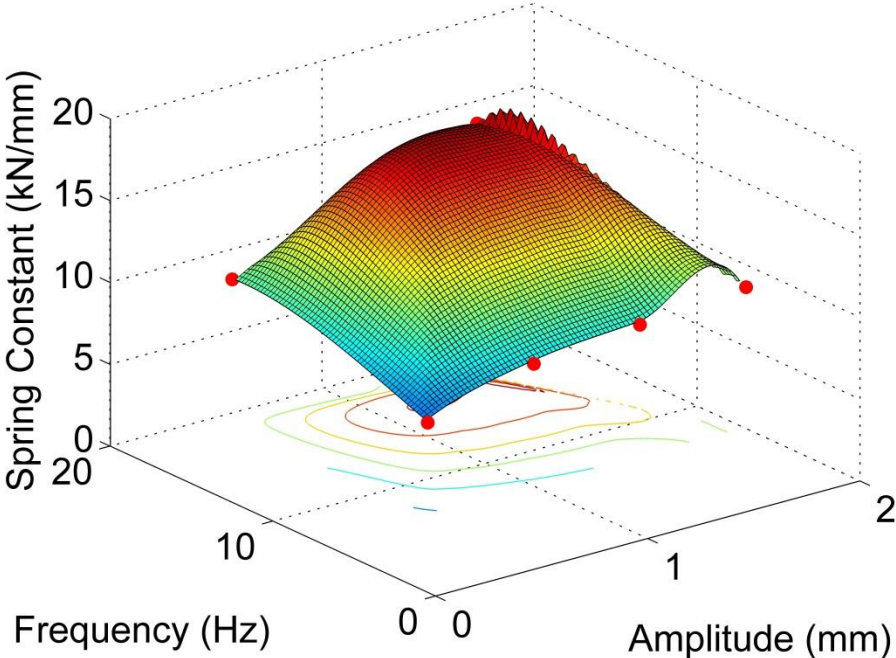


Figure 37 Change in the spring constant (KN/mm) with frequency (Hz) and Amplitude (mm)

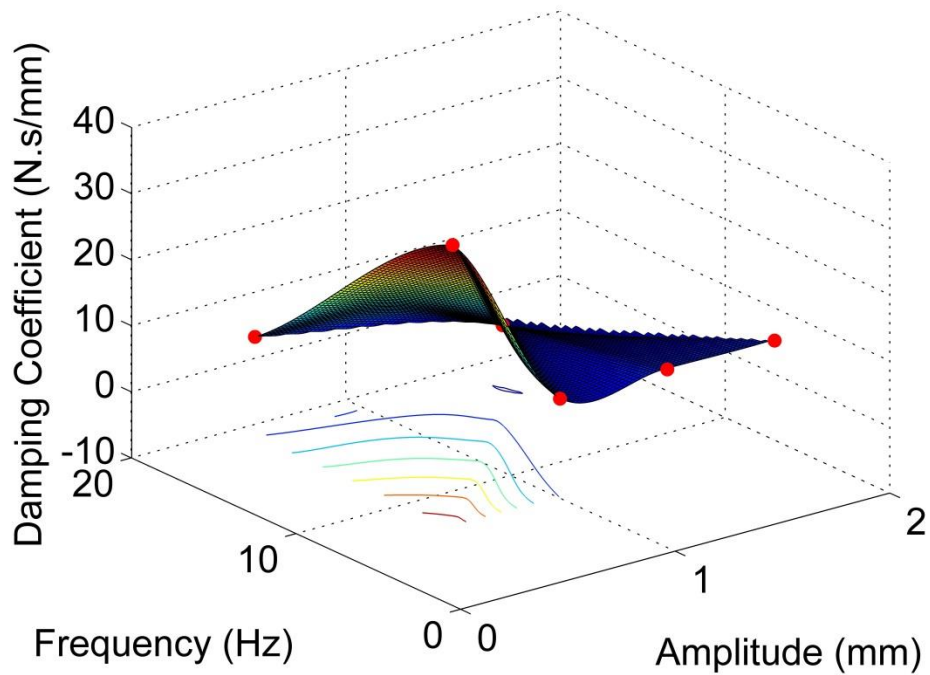


Figure 38 Change in the damping coefficient (N.s/mm) with frequency and amplitude

With frequencies from 4.5Hz up to 19 Hz and amplitude from 0.5 to 2 mm, we have the expressions to predict the spring constant and damping coefficient.

$$K = ax^2y^2 + bx^2y + cxy^2 + dx^2 + ex + fy^2 + gy + h$$

$$C = ax^2y^2 + bx^2y + cxy^2 + dx^2 + ex + fy^2 + gy + h$$

$$K = 0.432447315029147x^2y^2 - 9.22104802687009x^2y - 0.187426797489446xy^2 + 45.7521217849876 + 10.5745028936596x - 1.59593156133203y^2 + 43.8756755654609y - 224.766174602997$$

$$C = 0.0193532580888564x^2y^2 - 1.45253457142365x^2y + 0.150070291132485xy^2 + 40.4507306869378x^2 + -90.0960850988198x - 0.703365538232218y^2 + 14.6353075356960y - 3.95108387653934$$

In which x is the amplitude, y is the frequency.

The following are some examples of the tests data result of the springs and rubbers.

Table 8 The tests data result of the 6 rings springs

| Analysis result of the 6 rings springs data | | | |
|---|-------------|-----------------------|--------------------------|
| The amplitude and the frequency : | K (kN/mm) | Peak damping (N.s/mm) | Average Damping (N.s/mm) |
| Field work 6springs 7hz 2mm 1.5kn | 8.621898 | 8.41115 | 5.0299 |
| Field work 6springs 7hz 0.5mm 1.5kn | 5.621146 | 32.65945 | 5.086 |
| Field work 6springs 7hz 1.5mm 1.5kn | 8.086565 | 9.49945 | 5.06175 |
| Field work 6springs 7hz 1mm 1.5kn | 7.4554 | 6.09445 | 5.0294 |
| Field work 6springs 19hz 1mm 1.5kn | 8.2838 | 5.3225 | 5.0266 |
| Field work 6springs 19hz 0.5mm 1.5kn | 8.8754 | 6.80445 | 5.0294 |
| Field work 6springs 7hz 2mm 15kn | 24.259642 | 36.3892 | 5.02935 |
| Field work 6springs 7hz 1.5mm 17kn | 32.839353 | 27.51435 | 5.02794 |
| Field work 6springs 17hz 2mm 15kn | 28.59872311 | 33.5279 | 5.02795 |
| Field work 6springs 19hz 2mm 15kn | 27.21809 | 28.11955 | 5.1554 |
| Field work 6springs 17hz 1.5mm 19kn | 36.09369 | 26.9224 | 5.02925 |
| Field work 6springs 19hz 2mm 1.5kn | 11.834 | 7.4004 | 5.4004 |
| Field work 6springs 17hz 1.5mm 1.5kn | 14.79507 | 12.1316 | 5.29395 |
| Field work 6springs 19hz | 11.43958 | 9.7624 | 5.098 |

| | | | |
|---------------------------------------|----------|----------|---------|
| 1.5mm 1.5kn | | | |
| Field work 6springs 7hz 1.5mm 15kn | 15.67999 | 17.30115 | 5.02345 |
| Field work 6springs 7hz 2mm 15kn | 44.37732 | 47.0548 | 5.00985 |
| Field work 6springs 17hz 2mm 15kn | 22.48435 | 42.0213 | 5.01925 |

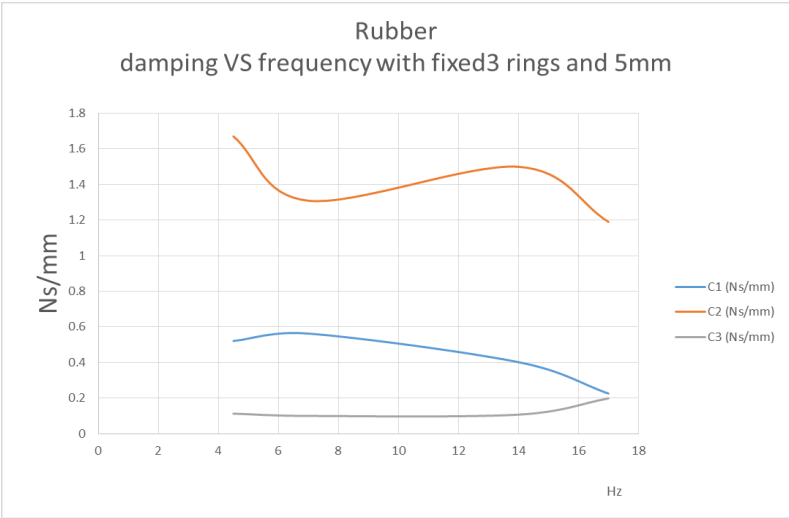


Figure 39 Three rubber O-rings test data under 5mm amplitude with different frequency

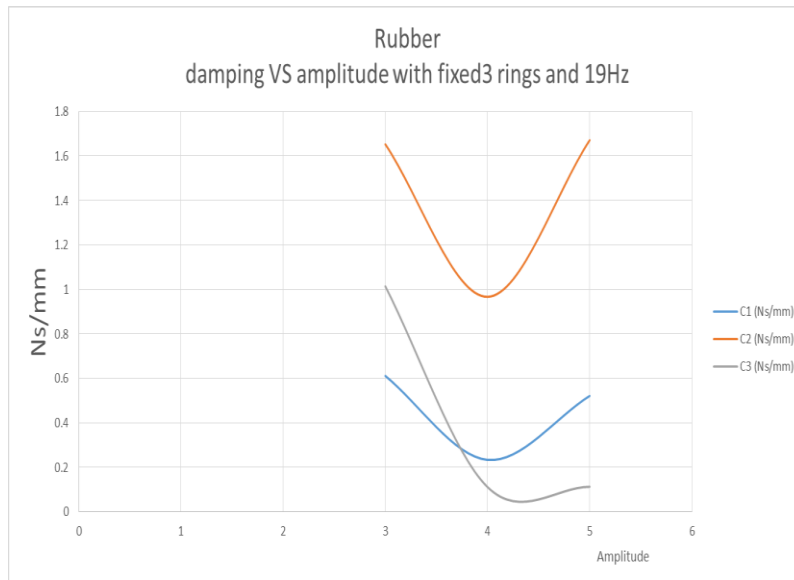
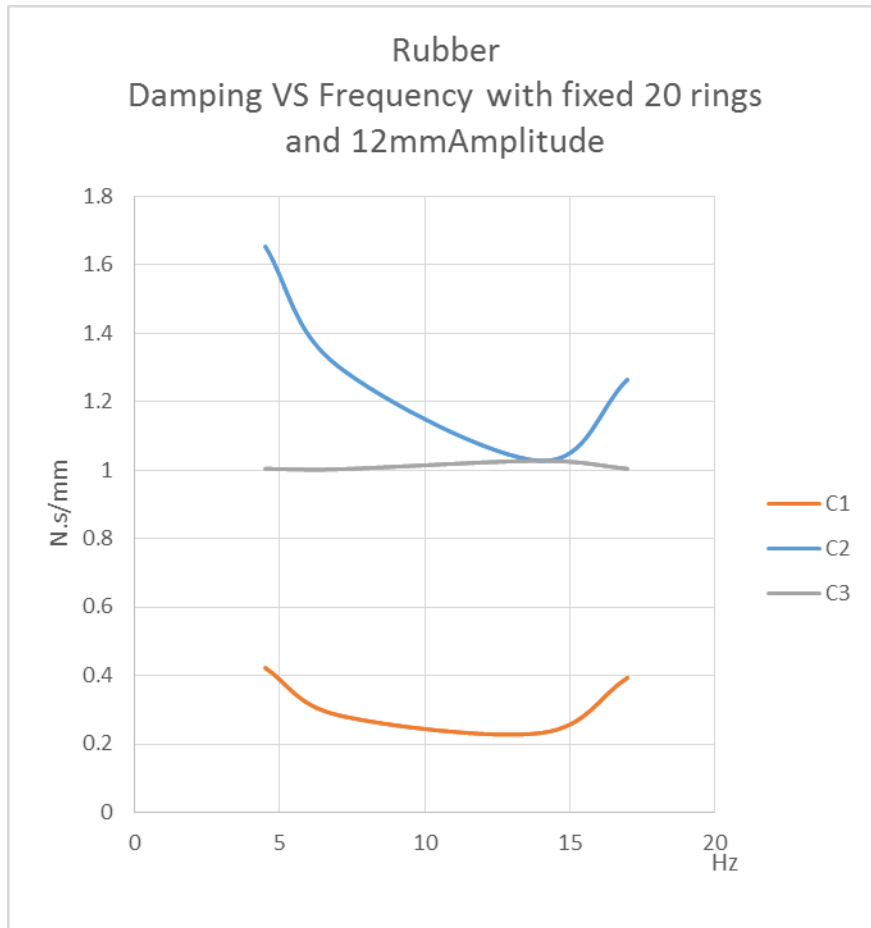


Figure 40 Three rubber O-rings test data under 19Hz with different amplitude

Comparing the Fig39 with Fig40, it is clearly shown that, in the rubber test, when the amplitude is within 5 mm and the frequency changes, there is no significant influence on the damping change. Note that 5 mm amplitude is reasonable for 3 rings. On the contrary, with a fixed frequency, once the amplitude changes from 3mm to 5mm, the damping has an obvious change. Consequently, finding the reasonable range of the amplitude is important. The rubber used in the field trail is 12.5 mm thick with 50% compression on it, based on the previous research. Hence, 12 mm amplitude is a wise choice to be selected for 20 rings. The result shows that it is really ideal and approximately close to the real field trail data for the test.



| Rubber | | | | |
|---------------------------|-----------|------------|------------|------------|
| | K (kN/mm) | C1 (Ns/mm) | C2 (Ns/mm) | C3 (Ns/mm) |
| 20 rings 4.5hz 12mm 28-8 | 0.031808 | 0.4224 | 1.654 | 1.0042 |
| 20 rings 7hz 12mm 28-9 | 0.032617 | 0.2845 | 1.3047 | 1.0029 |
| 20 rings 14 hz 12mm 28-10 | 0.032118 | 0.2319 | 1.0278 | 1.0276 |
| 20 rings 17hz 12mm 28-11 | 0.037203 | 0.3936 | 1.2649 | 1.0045 |

Figure 41 A classical calculation graph and data of the rubber's damping.

Fig41 shows that the 20rings rubber damping data and the C_3 is the average value of the damping coefficient. From the equation of the parallel rubbers damping, based on the 20 rubber rings damping, it can get the 24 rubber rings damping, which is the damping of the field trail rubber. Because in the design the rubbers and the springs are parallel, it added the springs'

stiffness in the future simulation too. The average damping was 2.0Ns/mm which means 2×10^3 Ns/m. It was put in the PFC2D simulation.

Both the frequency and amplitude can affect the spring constant. Preliminary test results in DTL field trial report shows that the amplitude was less than 1.5 mm for each rings. Hence, the amplitude was set as 1 mm. When the frequency is higher than 19Hz, the damping coefficient only depends on the frequency. Hence, the amplitude is eliminated from the equation when predicting the damping coefficient under this occasion.

6.2 Analysis and Conclusion

Hundreds of tests were conducted to find the spring stiffness and damping coefficient of the specific rubbers and springs under the reasonable range of the frequency and amplitude which consistently match with the new pVARD tool. The mainly frequency-dependent spring stiffness and the amplitude-dependent of the rubbers are set in the drilling machine, and are two important goals in the test. The pVARD tool is designed to generate the vibration with different frequencies, which could increase the rate of penetration in the drilling process. The test results were used to derive the equations for spring constant and damping coefficient. Then, these parameters were then used to calculate the transmitted force to the PDC bit and drill pipe, with a PFC model. From the result, it is shown that the springs let most of the generated force transmitted to the drill pipe, with some dynamic amplification. However, the damping of the rubber reduces the force to the PDC bit.

In the future, with many non-zero deflections, different material rubbers damping can be tested to improve the spring-damping model. Also, it is possible to improve the rock cutter interaction model by working on complexity and precision. This will lead to a better predictive model to test the performance of vibration force in the drilling engineering.

Chapter 7 DEM Modeling of the pVARD

Drilling Under Field Conditions

7.1 Field Trial Summary

In 2014, the Drilling Technology Laboratory at Memorial University conducted field drilling trials of several technologies that were developed at the lab, including the pVARD drilling tool, the SensorSub (a downhole logging-while-drilling tool), techniques to accurately measure bits wear and damage, dynamic drilling and drillstring vibration models, and seismic-while-drilling (SWD) applications. This work was done at Greenslades Construction Quarry in Conception Bay South, Newfoundland and Labrador where 3 vertical wells were drilled through shale formations ending in a basement of igneous rock, which was assumed to be granite. Figure 42 shows the drill rig, research personnel and some drilling tools on-site, while Figure 43 shows a plan of the field site and a geological section showing the formations penetrated by the 3 wells. The 2 main shale formations penetrated were the upper grey shale and the deeper red/green shale, both of which had estimated UCS of approximately 50 to 60 MPa. Further details of the field trial are given in the Field Trial Report [48].

For field drilling, the pVARD tool was mounted in the bottom-hole-assembly (BHA) near the bit and was used with a 152 mm diameter PDC Bit. Figure 44 outlines the typical BHA configuration used for pVARD drilling and Table 9 outlines the specifications of the PDC bit. For most drilling, drill-off-tests were conducted where the WOB was held constant over



Figure 42. The field drilling site showing the pVARD tool (left), the PDC drill bit (center) and the SensorSub (right). [48].

measured depth intervals of 1 to 3 m and then increased and held for the next WOB increment.

ROP was then calculated for each WOB increment.

Table 9. Specifications of the M716 PDC bit used in the field drilling [48]

| Design Specifications | |
|------------------------------|--------|
| Bit gauge diameter | 152 mm |
| Total cutters | 28 |
| Cutter size | 16 mm |
| Face cutters | 21 |
| Blade count | 7 |

| | |
|----------------------|-----------------------------------|
| Nozzles | 2 fixed ports, 3 adjustable ports |
| Range of WOB applied | 40KN to 140 KN |

During the field trial, the pVARD tool was evaluated using 3 different compliance settings by changing the configuration of the elastic springs, as summarized in Table 10. It was observed that the drilling ROP was increased when using the pVARD tool (as compared to drilling without the pVARD tool for drilling the same formations and at the same WOB) but only for some compliance settings. This is shown in Figure 45 for drilling in the red shale, which shows that for drilling with Configuration #2, the ROP is greater than conventional drilling over the range of 6000 to 10000 kg (60 to 100 kN) WOB, while ROP is no better than drilling without the pVARD tool (Conventional Drilling) for WOB above or below this range. Similarly, drilling with Configuration #1 showed no difference in ROP for pVARD and Conventional Drilling. Analysis of these results indicated that the pVARD tool increased ROP for the range of WOB

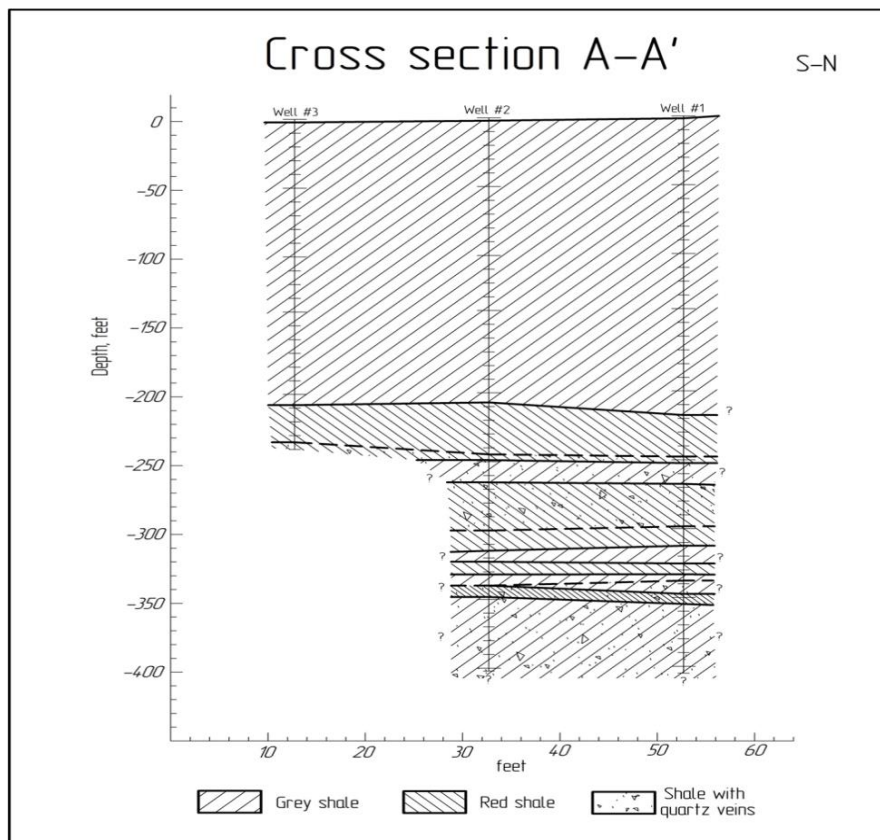


Figure 43. Geological section of the field site constructed from the well drill cuttings analysis. [48].

that corresponded with approximately 25% to 75% of the total spring closure or flat load. It was showed that within this optimal range, the pVARD tool kept the bit in good contact with the rock but had enough compliance to allow the cutters to vibrate axially due to the cutter actions. For WOB above this optimal range, the springs would be compressed to the point where axial vibrations would have low or even negligible amplitude and be the same as non p-VARD or conventional drilling. For WOB below the optimal range, the compliance would be too high and allow the bit to momentarily ride over the rock surface and reduce the penetration rate. The objective of the research outlined in this chapter was to test and evaluate this theory by specifically simulating the field trial drilling for pVARD configuration #2 (as shown in Figure 45) utilizing the DEM pVARD simulation methodology developed in Chapter 5 and the full scale pVARD tool compliance characterization given in Chapter 6.

Table10. pVARD tool configuration for the field trials.[48]

| S.no | Parameters | Values |
|------|-----------------------------|------------------------------------|
| 1 | O.D | 4 inch |
| 2 | I.D | 1 ¹ / ₄ inch |
| 3 | Length of tool | 12 ft. (Approx.) |
| 4 | Type of spring | Belleville spring washers |
| 5 | Number of springs | 30 |
| 6 | Dampening material | Neoprene rubber |
| 7 | Working load | 3120 lbs, 6240 lbs, 9360 lbs |
| 8 | Flat load | 4380 lbs, 8760 lbs, 13140 lbs |
| 9 | Deflections at working load | 1.68", 0.84", 0.56" |

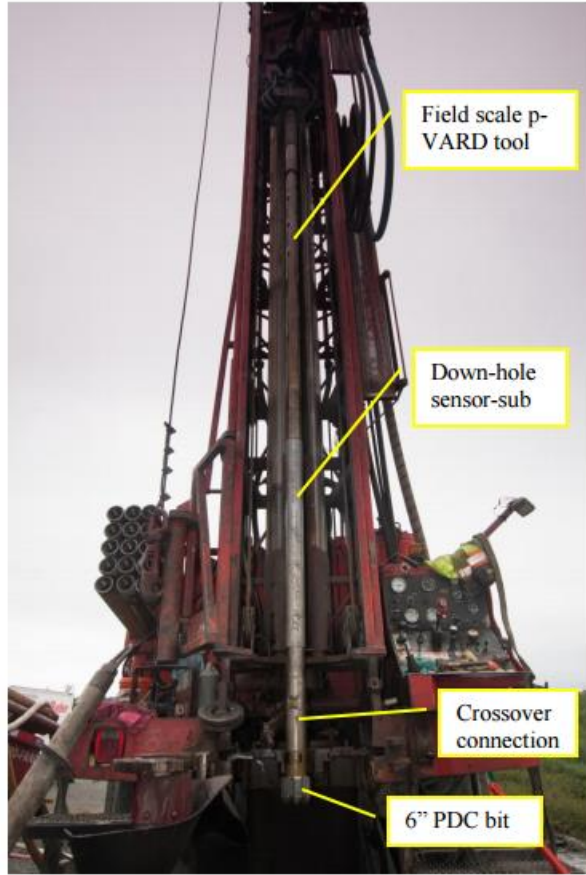


Figure 44. The pVARD tool Bottom Hole Assembly (BHA) for field trials [34]

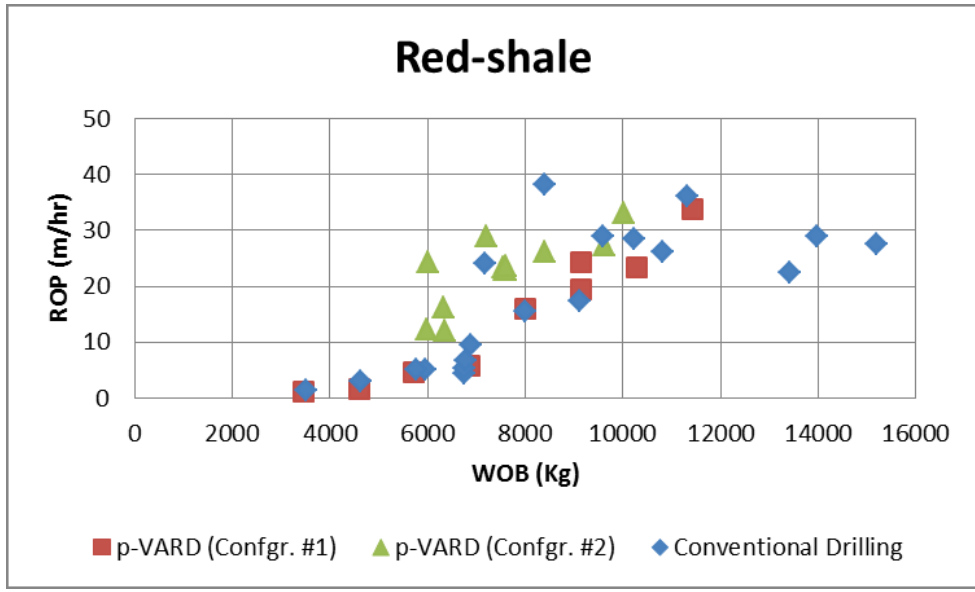


Figure 45 Drilling test results showing ROP for drilling in Red Shale with various pVARD and non p-VARD configurations. [34]

7.2 DEM Input Data

The parameters needed for the pVARD tool simulation are outlined in Chapter 5 dealing with the lab scale pVARD tool simulation. To simulate the field scale pVARD drilling, the same DEM parameters were used but adjusted to match the field scale pVARD tool (Configuration #2) and the field trial drilling data, both as shown in Figure 45. The determination of these simulation parameters is given below.

Non varying Drilling Parameters

- Rotary Speed = 80 rpm
- Rock strength = 50 MPa
- Bit hydraulics cleaning efficiency = 100%

Bottom-hole Pressure

For the drilling data given in Figure 45, the bottom-hole pressure averaged approximately 200 psi. However, it was important to conduct the simulations at lower BHP, including drilling under atmospheric conditions, and at higher BHP to predict performance at greater depths than encountered in the field trials. Therefore, BHP were used with values of 0, 100, 200, 500 and 1000 psi.

Vertical Cutter Forces

As outlined in Chapter 5, there is one static component and two dynamic components of the vertical force applied to the cutter:

- 1) Static WOB: $F_1=mg$, where m is the buoyant mass of the drill string and g is gravity;
- 2) pVARD damping force: $F_2=Cv$, where C is the damping coefficient and v is cutter y-velocity;
- 3) pVARD spring force: $F_3=Kx$, where K is the spring stiffness and x is the spring displacement.

From the range of WOB used in the field trial, as shown in Figure 44 the values of WOB used were 40, 60, 80, 100, 120, and 140 kN. From the dynamic characterization of the damping material in Chapter 6, a damping coefficient of $C = 3 \times 10^3$ Ns/m was used. For pVARD configuration #2, 30 Belleville springs were used, so the corresponding spring stiffness was calculated using $\frac{1}{K_{total}} = \frac{1}{K_1} + \frac{1}{K_2} + \frac{1}{K_3} + \dots + \frac{1}{K_{30}}$, which gives $K \approx 1.5$ kN/mm.

7.3 DEM Simulation Results

DEM results were analysed following the methodology given in Chapter 5 and given as MRR, MSE and ROP at each combination of WOB and BHP for both pVARD and Rigid (non pVARD) conditions. Figures 46a and 46b compare the results of the pVARD and Rigid drilling results on the same graphs. These results show that pVARD drilling is improved relative to rigid drilling for WOB of 60, 80 and 100 kN, with higher MRR and ROP, and lower MSE. For WOB below or above this range (40, 120, and 140 kN), there is essentially no difference between the pVARD and Rigid drilling. These results agree closely with the pVARD field data shown in Figure 46, which shows higher pVARD ROP for WOB of 60, 80 and 100 kN (6000, 8000 and 10000 kg in Figure 46(a)) and essentially no difference for WOB above or below this range (10000, 12000 and 14000 kg in Figure 46(a)). As expected, ROP and MRR decrease and MSE increases with increasing BHP, however, the improvement in pVARD drilling within the optimal range of WOB occurs for all values of BHP.

Figure 47 presents the same data arranged with all WOB curves for pVARD and Rigid results on the same graph. Evaluation of this data shows the same observation as for Figure 46(a) and 46(b), namely that pVARD drilling is improved relative to Rigid drilling for WOB of 60, 80

and 100 kN, and essentially the same for other WOB. Once again this agrees with the field drilling trial results given in Figure 45.

Overall, these results suggest that the DEM simulations have captured the same bit-rock interactions as the pVARD field drilling with a similar net influence on drilling penetration rate and specific energy. Further evaluation of this is the focus of future research.

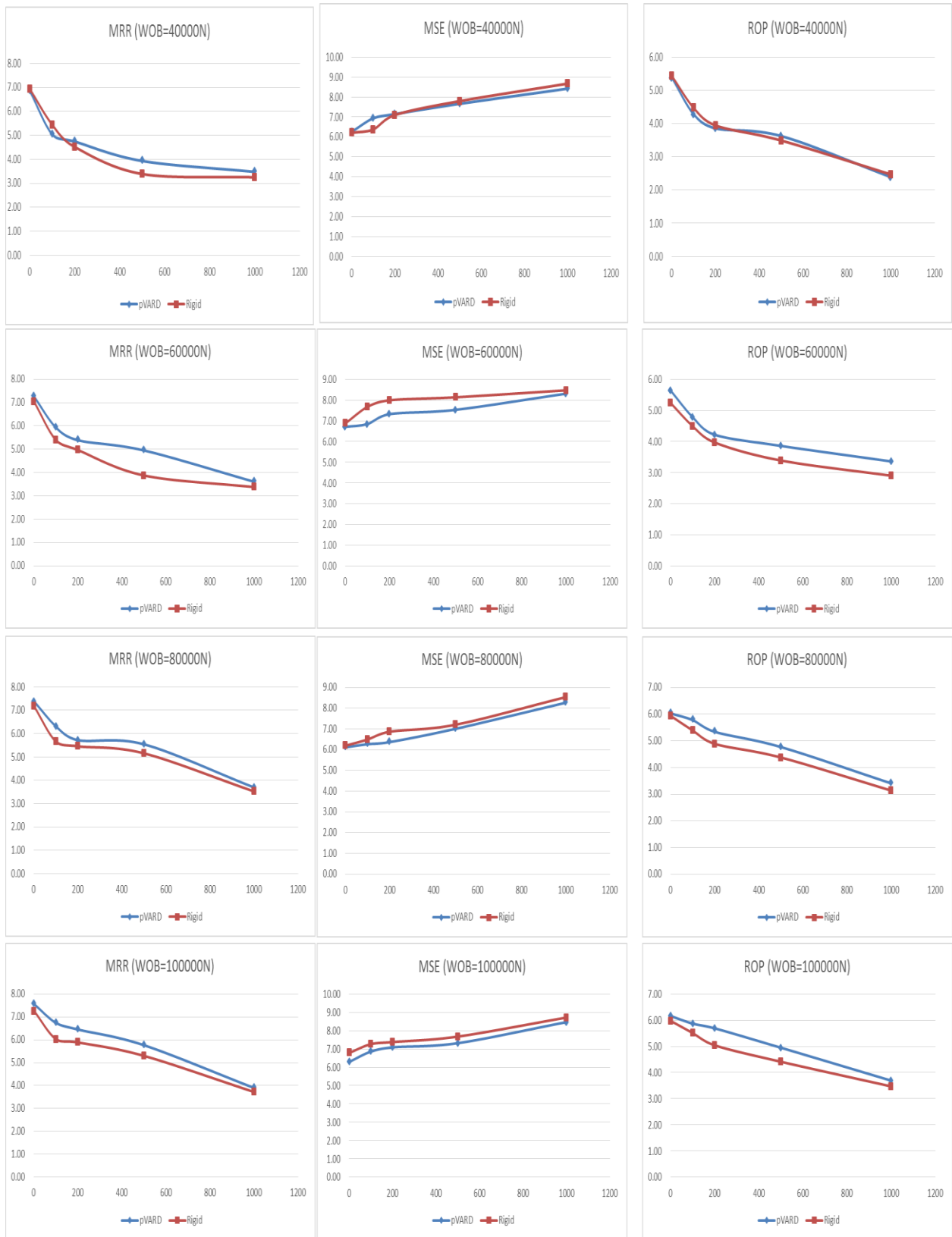


Figure 46(a) MRR, MSE and ROP for WOB of 40, 60, 80, and 100 kN and bottom-hole pressure ranging from 0 to 1000psi. MRR, MSE and ROP are in units of $10^{-3} \text{ m}^3/\text{s}$, KJ/m^3 , and $10^{-2} \text{ m}/\text{s}$, respectively.

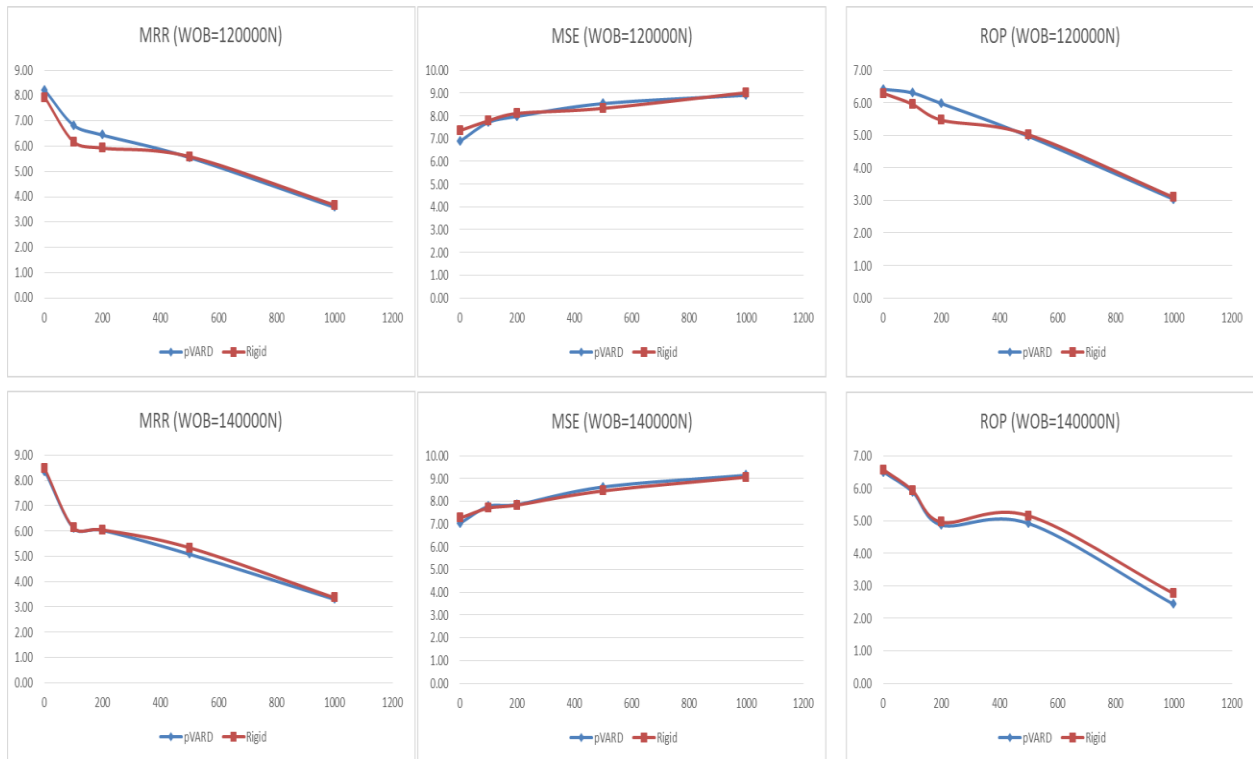


Figure 46(b) MRR, MSE and ROP for WOB of 120 and 140 kN and bottom-hole pressure ranging from 0 to 1000psi. MRR, MSE and ROP are in units of $10^{-3} \text{ m}^3/\text{s}$, KJ/m^3 , and $10^{-2} \text{ m}/\text{s}$, respectively.

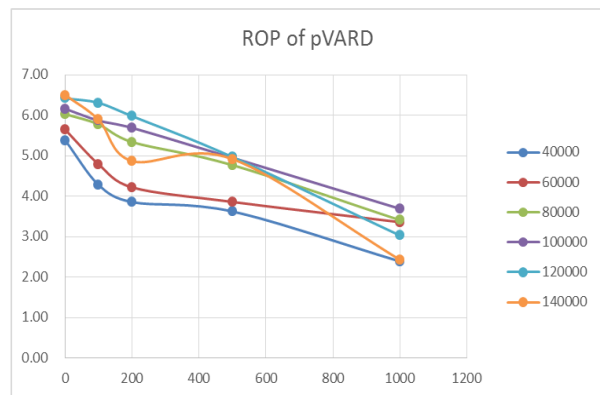
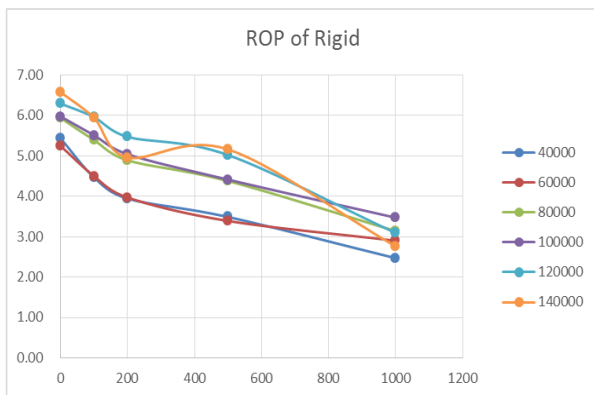
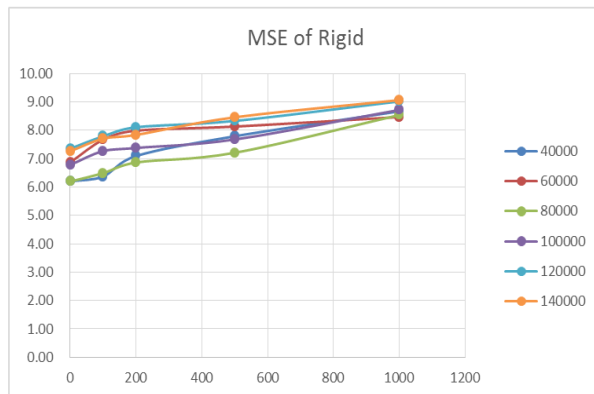
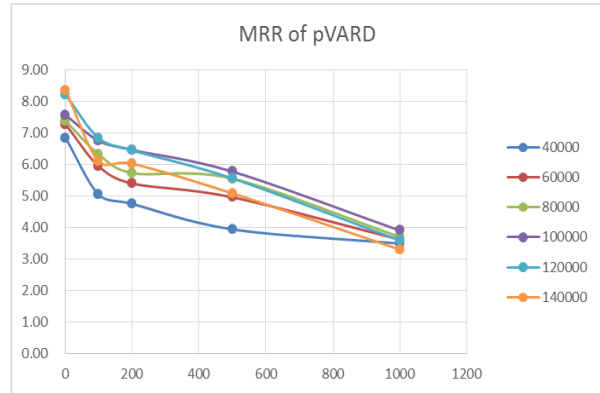
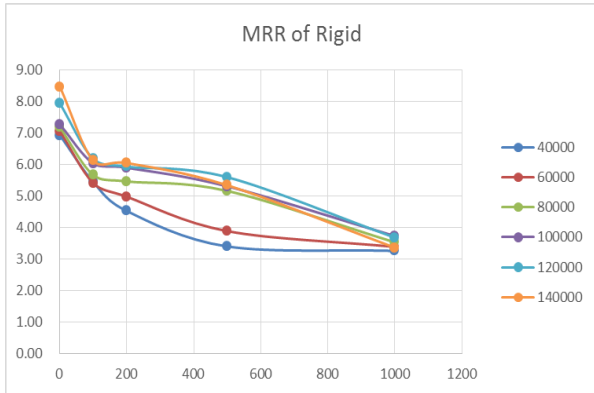


Figure 47 Comparison of MRR, MSE and ROP for rigid and pVARD drilling at all WOB and bottom-hole pressures. MRR, MSE and ROP are in units of $10^{-3} \text{ m}^3/\text{s}$, KJ/m^3 , and $10^{-2} \text{ m}/\text{s}$, respectively.

Chapter 8 Conclusion and Future Work

8.1 Summary and Conclusion

This final chapter is about the conclusions and future work of the rock cutter interaction and the pVARD tool simulation. The results will also be compared. The process of the rock cutter interaction is simulated and investigated. The vibration force on the cutter has changed with different weight on bit, damping coefficient, spring stiffness and bottom-hole pressure. The simulation result demonstrated that the impacting velocity within a certain range (X-velocity and rigid tool Y-velocity) has less effect on the cutting force. The variation of the vibration force is unanimous to rock volume changes with stepwise decreasing, such as the changing of MRR and average ROP.

In this thesis, two drilling tools are simulated and compared, which are pVARD tool and rigid (no vibration) drilling tool. Meanwhile, the field trial and lab tests were all conducted during this research time. The purpose of the simulation is to compare the performance of the new pVARD tool on some of the key factors, such as the rate of penetration (ROP), the Depth of Cut (DOC), Mechanical Specific Energy (MSE) and Material Removal Rate (MRR). Moreover, another purpose is to analyze the axial compliance, which comes from the pVARD tool during the drilling process, such as the damping coefficient of the rubber and the spring stiffness of the O-rings springs in the tool. Finally, the most significant outcome of this research and simulation is to get the boundary of the pVARD tool use and provide a directive standard which cannot get in the field work to pVARD tool user in the future. The simulation result is discussed and analyzed.

According to the simulation result the pVARD tool has an obviously higher average ROP and MRR performance than the rigid (no vibration) tool under the reasonable drilling WOB and bottom-hole pressure.

8.1.1 Axial Compliance and Effect of PVAR Tool

As mentioned above, axially compliant section and energy absorbing section in the pVARD tool equipment are most important factors influencing the drilling performance. From this two sections, damping and spring vibration tool is generally useful when keeping the drill string from the PDC bit. It means that the pVARD tool has the Bruna-N rubber rings and springs tool, which has axial compliance and absorbing the extra energy, while the previous rigid tool does not. In order to analyze the axial compliance from the springs and rubber, extra simulations and lab tests were conducted. The other parameters keep the original values, such as load and frequency on the materials. Finally, except the simulation for the tool itself, the author built the relationship between the amplitude, frequency, spring stiffness and the damping coefficient. It not only provide a real simulation parameters for the PFC simulation approximately near the experiments, but also give a reference value to the future pVARD tool work and simulation.

8.1.2 Conclusion

In this thesis, two drilling tools are simulated and compared, which are pVARD tool and rigid (no vibration) tool both under lab scale and field trial real scale work. The parameters of the simulation environment are the real data from lab experiment and field work trial. The simulation environment is built using PFC2D modelling tool. Some important parameters are

calculated by the author before input, such as spring stiffness and damping coefficient. Meanwhile, the field trial and lab were all conducted by DTL group. In the simulation, the WOB are kept at 40KN, 60KN, 80KN, 100KN, 120KN and 140KN respectively, but the bottom-hole pressure increases with the values of 0, 100, 200, 500, 1000psi. Then the MSE is increased with the bottom-hole pressures but the pVARD tool is increase much smaller than the no tool simulation. At the same time, MRR and ROP values above are also simulated for each different WOB. During the idea range of the 60000N to 100000N, the ROP and MRR values show that the pVARD tool could directly improve the drilling performance which agrees with the field work test. It is the significant contribution of the author during this two years research, no matter work in the lab, field trial or computer room overnight every work days. It provide a new tool and new simulation method could use in the bit rock interaction study.

8.2 Future work

In this PFC simulation the author only used the medium strength rocks, which similar with the red shale in the CBS, NL field trial and concrete samples in the DTL lab. However, in the future this simulation could expand to the higher or lower strength and different types and characteristics of rocks. Meanwhile, as the development of the software, not only the PFC2D, the new DEM simulation software like PFC3D or even the FDEM simulation software also could use in the drilling engineering bit rock interaction simulation.

Appendix A

MSE and MRR and Average ROP Calculation

a) MSE Value Calculation

MSE is amount of energy consumed to remove specific volume of rock. According to the classic theories and formulas of the energy and force:

$$W = F*d \quad (1)$$

Where W represents the amount of work that is done by force F over a length of d.

The MSE value computational process could be separated into two different methods.

The first one is for the experiment, which related to the torque:

$$MSE = \frac{WOB}{A_b} + \frac{2 \pi * RPM * Torque}{A_b * ROP} \quad (2)$$

Where: MSE = Mechanical Specific Energy (psi)

WOB = Weight On Bit (lb)

RPM = Rotations Per Minute

Torque = Rotational torque (in-lb)

A_b = Cross sectional area of bit (in²)

ROP = Rate of Penetration (in/hr)

For the general condition and the simulation part, every time-step the amount of energy consumed on the cutter is calculated using cutter displacement and amount of force applied on the cutter. They all were set up and calculated in the PFC2D simulation. At the end of the process, total energy consumed over the entire process is calculated. Using this energy and the removed volume that was calculated, the MSE value can be calculated as follow:

$$MSE = \frac{\text{Total energy consumed}}{\text{Total amount of rock volume removed}} ; (3)$$

So, in the simulation, MSE is:

$$MSE = \frac{\text{Energy of the work done in Cutting Action}}{\text{Volume of Rock Cut}} = \frac{\int(\text{Force})dx}{\text{Volume of Cut}} = \frac{\sum_{t_1}^{t_2} F_x \cdot \Delta X}{Z \cdot \sum_{t_1}^{t_2} Y \cdot \Delta X} \quad (4)$$

b) MRR Value

For MRR value calculation, it used a method similar to differential and integration in calculus. First, it needs to calculate the total area of cutting. By recording the vertical(Y-position) and horizontal (X-position) position of the cutter, it could simply compute the area of every minimum time span. Then, by adding up all the small unit areas, there is the value of cutting area. Hence, the MRR value can be computed by dividing the volume by time-step length. The simply volume calculation for a bulk is base times height which is: $a \cdot b \cdot h$. Using Excel worksheet, all of the rectangles are then added up to calculate the total volume of removed rock over a specific period of simulation time. Dividing this volume by drilling time, the MRR value for the process is calculated.

$$\text{MRR} = \frac{\text{Total amount of rock volume removed}}{\text{Total time}} \quad (5)$$

Due to the number of data point (time-step) exceed 400000 especially in the field work simulation, both MSE and MRR values for the different simulation runs are calculated using Excel sheet, and then output in the Matlab and process in the Matlab code. Since the time-step is in a pretty short flash, the simulated result shows that the MSE and MRR parameters is close to the real value, which meet the demand for measuring precision.

REFERENCES

- [1] I. C. G. Inc., "Particle Flow Code Manual 4th edition," 2008.
- [2] Schlumberger PDC Smith Bits Data Sheet. Retrieved from www.slb.com/pdc.
- [3] Detournay, "A phenomenological model for the drilling action of drag bits," *International journal of rock mechanics and mining sciences & geomechanics abstracts*, vol. 29, pp. 13-23, 1992.
- [4] Detournay, "Drilling response of drag bits: theory and experiment," *International Journal of Rock Mechanics and Mining Sciences*, vol. 45, pp. 1347-1360, 2008.
- [5] Gerbaud, "PDC bits: all comes from the cutter rock interaction," in *IADC/SPE Drilling Conference*, 2006.
- [6] L. W. Ledgerwood, "Efforts to Develop Improved Oilwell Drilling Methods," *Journal of Petroleum Technology*, vol. 12, no. 4, pp. 61-47, 1960.
- [7] A. T. Bourgoyne Jr, K. K. Millheim, M. E. Chenevert and F. S. Young Jr, *Applied Drilling Engineering*, Richardson TX: Society of Petroleum Engineers.
- [8] Wikipedia Shi, G, Discontinuous deformation analysis – A new numerical model for the statics and dynamics of deformable block structures, 16pp. In 1st U.S. Conf. on Discrete Element Methods, Golden. CSM Press: Golden, CO, 1989.
- [9] Akbari, Babak, 2011. "Polycrystalline diamond compact bit-rock interaction"
- [10] Khorshidian, H. 2012. Phenomena Affecting Penetration Mechanism of Polycrystalline Diamond Compact Bit. Master's dissertation, Memorial University of Newfoundland, St.

John's.

- [11] M. Mozaffari, Comprehensive simulation of single PDC cutter penetration using distinct element modeling (DEM) methods, 2013 Master's thesis, Memorial University of Newfoundland, St. John's.
- [12] Yousef Gharibiyamchi, Evaluation and Characterization of Hydraulic Pulsing Drilling Tools and Potential Impacts on Penetration Rate, 2013 Master's thesis, Memorial University of Newfoundland, St. John's.
- [13] Ranman K E, A model describing rock cutting with conical picks[J]. *Rock Mechanics and Rock Engineering*, 1985, 18(2): 131—140.
- [14] Copur H, Bilgin N, Tuncdemir H, Balci C. A set of indices based on indentation tests for assessment of rock cutting performance and rock properties[J]. *The Journal of the South African Institute of Mining and Metallurgy*, 2003, 103(9): 589—599.
- [15] Biligin N, Demircin M A, Copur H, et al. Dominant rock properties affecting the performance of conical picks and the comparison of some experimental and theoretical results[J]. *International Journal of Mining Engineering*, 2006, 43(1): 139—156.
- [16] Evans, I., A theory of the picks cutting force for point-attack, *International Journal of Mining Engineering*, 2(1) (1984) 63-71.
- [17] Roxborough, F.F, Liu, Z.C., Theoretical considerations on pick shape in rock and coal cutting. *Proceedings of sixth underground operator's conference, Australia*, (1995) 189-193.
- [18] Goktan, R. M., A suggested improvement on Evans's cutting theory for conical bits, *Proceedings of fourth symposium on mine mechanization automation*, 1 (1997) 57-61.

- [19] L. Ledgerwood III, "PFC modeling of rock cutting under high pressure conditions," in 1st Canada-US Rock Mechanics Symposium, 2007.
- [20] F. Vajdova, "Compaction, dilatancy, and failure in porous carbonate rocks," *Journal of Geophysical Research: : Solid Earth*, 2004.
- [21] B. P. Wong, "Mechanical compaction of porous sandstone," *Oil & Gas Science and Technology*, pp. 715-727, 1999.
- [22] M. Mozaffari, *DEM Modeling of Bit/Rock Interaction: An Overview of the Developed PFC2D Toolkit*, 2013.
- [23] Reyes, R., Kyzym, I., Rana P.S., Molgaard J. and Butt, S.D, *Cuttings Analysis for Rotary Drilling Penetration Mechanisms and Performance Evaluation* in ARMA 15-764 Memorial University of Newfoundland, St. John's, NL, Canada
- [24] Resonantsonic Drilling Innovative Technology Summary Report. Prepared for US Department of Energy. 1995.
- [25] Eskin, M., W.C. Maurer and A. Leviant. 1995. Former-USSR R&D on Novel Drilling Techniques. Maurer Engineering Inc.
- [26] G. L. McCarthy, "A Step Change in Drilling Efficiency: Quantifying the Effects of Adding an Axial Oscillation Tool within Challenging Wellbore Environments," in *SPE/IADC Drilling Conference and Exhibition*, 2009.
- [27] Li, H. 2011. Experimental investigation of the rate of penetration of Vibration Assisted Rotary Drilling. Master's dissertation, Memorial University of Newfoundland, St. John's.
- [28] Khorshidian, H. 2012. Phenomena Affecting Penetration Mechanism of Polycrystalline

- Diamond Compact Bit. Master's dissertation, Memorial University of Newfoundland, St. John's.
- [29] Butt, S.D., P.N Calder. 1998. Experimental Procedure to Measure Volumetric Changes and Microseismic Activity During Triaxial Compression Tests. *Int. J. Rock Mech. Min. Sci.* 35(2): 249-254.
- [30] Cai, M., P.K. Kaiser, Y. Tasaka, H. Kurose, M. Minami and T. Maejima. 2008. Numerical Simulation of Acoustic Emission in Large-scale Underground Excavations. In *The 42nd US Rock Mechanics Symposium (USRMS)*. American Rock Mechanics Association.
- [31] Keshavarz, M., F.L. Pellet K.A. Hosseini. 2009. Comparing the Effectiveness of Energy And Hit Rate Parameters of Acoustic Emission For Prediction of Rock Failure. In *ISRM International Symposium on Rock Mechanics-SINOROCK 2009*. International Society for Rock Mechanics.
- [32] Damani A., A. Sharma, C.H. Sondergeld and C.S. Rai. 2012. Mapping of Hydraulic Fractures under Triaxial Stress Conditions in Laboratory Experiments using Acoustic Emissions. In *SPE Annual Technical Conference and Exhibition, 2012, San Antonio, Texas*.
- [33] Khorshidian, H., S.D. Butt and F. Arvani. Influence of High Velocity Jet on Drilling Performance of PDC Bit under Pressurized Condition. *Proceedings of 48th US Rock Mechanics / Geomechanics Symposium, Minneapolis, MN, USA, 1-4 June 2014*.
- [34] Rana, P.S, A.N. Abugharara, S.D. Butt and J. Molgaard. Experimental and Field Application of Passive-Vibration Assisted Rotary Drilling (p-VARD) Tool to Enhance Drilling Performance. To be published in proceedings of 49th US Rock Mechanics / Geomechanics Symposium held in San Francisco, CA, USA, 28 June- 1 July, 2015.

- [35] ASTM D6913-04. Standard Test Methods for Particle-Size Distribution (Gradation) of Soils Using Sieve Analysis. ASTM International, West Conshohocken, PA, 2009, www.astm.org.
- [36] ASTM D422-63. Standard Test Method for Particle-Size Analysis of Soils. ASTM International, West Conshohocken, PA, 2007, www.astm.org
- [37] Moad, D., Mclellan, G., Wise, J., Barrow, J., Biancosino, D., Write, J. 1995. Resonantsonic Drilling-Innovative Technology Summary Report. US Department of Energy.
- [38] Li, H., Butt, S. D., Munaswamy, K. and Farid, A. "Experimental Investigation of Bit vibration on rotary drilling Penetration rate" ARMA 10-426, 44th US ROCK Mechanics Symposium and 5th US-Canada Rock Mechanics Symposium, Salt Lake City, June 27-30, 2010.
- [39] Khorshidian, H., Mozaffari, M. and Butt, S. D. (2012) "The Role of Natural Vibrations in Penetration Mechanism of a single PDC cutter", ARMA 12-09, Proceedings of 46th US Rock Mechanics/Geomechanics Symposium, Chicago, IL, US, 24-27 June 2012.
- [40] Teale, R. 1965. The Concept of Specific Energy in Rock Drilling. *Intl. J. Rock Mech. Mining Sci.* 2: 57-53
- [41] Khorshidian, H., Butt, S. D. and Arvani, F. (2014) "Influence of High Velocity Jet on Drilling Performance of PDC bit under Pressurized Condition, 48th US Rock Mechanics/GeoMechanics Symposium, Minneapolis, MN, USA.
- [42] Akbari, B., Butt, S. D., Munaswamy, K., & Arvani, F. (2011, January). Dynamic Single PDC Cutter Rock Drilling Modeling and Simulations Focusing on Rate of Penetration Using Distinct Element Method. In 45th US Rock Mechanics/Geomechanics Symposium, San Francisco, CA (pp. 11-379).

- [43] Xiao, Y., Zhong, J., Hurich, C. and Butt, S.D. 2015. Micro-Seismic Monitoring of PDC Bit Drilling Performance during Vibration Assisted Rotational Drilling. Proceedings of 49th US Rock Mechanics / Geomechanics Symposium, San Francisco, CA, USA.
- [44] Rafatian, N., Miska, S. Z., Ledgerwood, L. W., Yu, M., & Ahmed, R. 2009. Experimental study of MSE of a single PDC cutter under simulated pressurized conditions. In SPE/IADC Drilling Conference and Exhibition. Society of Petroleum Engineers.
- [45] Rafatian, "Experimental study of MSE of a single PDC cutter under simulated pressurized conditions," in SPE/IADC Drilling Conference and Exhibition, 2009.
- [46] K. R. Newman, G. T. Burnett, . J. C. Pursell and O. Gouasmia, "Modeling the Effect of a Down-hole Vibrator," in SPE/ICoTA Coiled Tubing & Well Intervention Conference and Exhibition, The Woodlands, Texas, 2009.
- [47] K. Emtehani Jahromi, G. Rideout, F. Arvani, S. Butt "Experimental Characterization of a Tubber Isolator for Dynamic Simulation of Vibration Attenuation in a Sonic Head Drilling Machine"
- [48] December 2014, Drilling Field Trial Report Edited by: P. S. Rana and Dr. S. D. Butt